Stony Brook University

MATERIAL CHARACTERIZATION OF HEALTHY AND OSTEOPOROTIC RAT FEMUR BONE

A Thesis Presented

by

KAUSHIK CHAVA

to

The Graduate School

in Partial Fulfillment of the

Requirements

for the Degree of

Master of Science

in

Materials Science and Engineering

Stony Brook University

May 2013

Stony Brook University

The Graduate School

KAUSHIK CHAVA

We, the thesis committee for the above candidate for the
Master of Science degree, hereby recommend
acceptance of this thesis.

T.A. Venkatesh
Assistant Professor
Department of Materials Science and Engineering

Yizhi Meng
Assistant Professor
Department of Materials Science and Engineering

Tadanori Koga
Associate Professor
Department of Materials Science and Engineering

This thesis is accepted by the Graduate School

Charles Taber
Interim Dean of the Graduate School

Abstract of the Thesis

MATERIAL CHARACTERIZATION OF HEALTHY AND OSTEOPOROTIC RAT FEMUR BONE

by

KAUSHIK CHAVA

Master of Science

in

Materials Science and Engineering

Stony Brook University

2013

Bone is a bio composite material made of organic and inorganic components. This unique material composition supported by hierarchical level structure enables it to perform wide range of activities and functions in human body. The inorganic phase consists of hydroxyapatite mineral crystals and the majority of organic phase is made of collagen fibers. A mineralized collagen fiber is the basic building unit in the structure of bone. The ability of bone to fine-tune its structure according to mechanical stress and repair its damaged regions differentiates it from modern synthetic materials. The bone modelling and remodeling is a very complex process which includes a high degree of synchronous effort from various factors and elements. Bone cells like Osteoblasts, Osteoclasts, Osteocytes and Bone lining cells are responsible for bone remodeling and intercellular signaling.

The mechanical behavior of bone varies between different hierarchical levels of bone structure. The architecture of bone matrix enables it to absorb maximum loads without breaking. Micro cracks developed during compressive loading within lamella helps in deflecting crack propagation. Several bone diseases are caused due to the lack of synchronous effort from the different factors involved in bone remodeling. Osteoporosis is caused due imbalance in activity of osteoblasts and osteoclasts which results in deteriorating microarchitecture of bone matrix. The patients with

osteoporosis experience a higher risk for bone fracture due to decrease in bone mineral density. It is more prevalent in elder women after menopause.

The effect of aging and osteoporosis on bone micro – structure and chemical composition are analyzed. A possible interrelationship between microstructure and chemical composition of bone samples is also studied. Healthy and osteoporotic bone samples of female Sprague – Dawley rats of 6 month and 12 month age groups are collected and characterized for topographical and chemical analysis. A High Resolution Analytical SEM (HRSEM) and Atomic Force Microscope are used for high resolution imaging for topographical information. HRSEM is also used for EDS analysis and quant mapping to determine the distribution of different elements. The AFM analysis has shown an increase in grain size for 12 month age group sample compared to their 6 month age group counterparts. The healthy bone samples have more aligned grains structure while the osteoporotic bone samples have more chaotic arrangement. The elemental distribution did not change much for an osteoporotic bone sample compared to healthy bones. A key observation from chemical analysis data is the decrease in magnesium content with bone aging.

Table of Contents

LIST OF FIGURES

LIST OF TABLES

Acknowledgments

I am deeply indebted to my research guides Dr. T.A. Venkatesh and Dr. Yizhi Meng for their support and guidance throughout the project. I would like to thank them for accepting me to be part of their research group and believing in me the entire duration. The time spent with the group has been an enriching and memorable experience.

A special note of thanks to Dr. Yizhi Meng for guiding and helping me in carrying out research at Brookhaven National Laboratory (BNL). The time bound approach and valuable suggestions of Dr. T.A. Venkatesh have also been pivotal in completion of the thesis.

I would like to express my gratitude to Derek Rammelkamp, my fellow group member for helping me on various occasions during this process. His support during research days at BNL is greatly appreciated, without which it would have been very difficult to complete the project in time.

I would also like to thank Xiao Tong and Fernando Camino for training me on Atomic Force Microscope and Scanning Electron Microscope equipment at BNL. Their tips and suggestions are very useful in obtaining better results.

Most importantly, I would like to thank all my friends and family members for their encouragement and support. Special mention for my parents, Rama Mohan Rao Chava and Jayanthi Chava for their love and support during rough days.

1. INTRODUCTION

Bone is an important organ in a human body performing several vital functions such as providing structure to the body, protecting internal organs and being responsible for locomotion. They also act as storage places for fatty acids, growth factors and minerals like calcium and potassium [1] [2]. It undergoes heavy dynamic loads and the structure, composition of bone plays a crucial role in withstanding these loads [3]. Bone is a bio – composite material made of organic and inorganic phases. The volumetric composition of bone is reported as 33 – 43% inorganic and 32 – 44% organic while the remaining 15 – 20% is occupied by water [4] [5]. It has a very complex structure with different hierarchical levels of organization [5].

The connective tissue which forms the bone matrix is called as osseous tissue or bone tissue. The bone tissue is divided into compact and spongy based on the type of bone they develop. The innermost part of bone is occupied by Trabecular (spongy bone) and is surrounded by Cortical (compact) bone as a shell. Both these bone types are different in their structure and mechanical properties. Compact bone is a hard and dense type of bone with porosity less than 10%. It provides the strength, stiffness and consists of 80% of total bone mass [6]. Compact bone consists of longitudinal channels along the length of the bone running parallel to its surface. These are called as haversian or central canals which consist of blood vessels and nerve cells. These channels are interconnected through Volkmann's or perforating canals and form a network within the bone matrix. This network plays a crucial role in transportation of blood, nutrients and minerals [7].

Trabecular (spongy) bone is predominantly located towards the end regions of a long bone called as Epiphysis. Epiphysis is the region close to the joints and the middle part of long bone is called Diaphysis. Spongy bone has an open structure with porosity of 80 – 90% and lacks the mechanical strength of compact bone. It is a weak and soft form of bone [6]. The pores are not well defined as compact bone and are filled with bone marrow. Bone marrow is responsible for blood cell

production through a process called as hematopoiesis. It also contains different types of bone cells, progenitor cells, nutrients and minerals. Spongy bone is very conducive to bone metabolism such as exchange of calcium ions due to its high porosity and proximity to bone marrow. Spongy bones also have higher surface ratio compared to compact bone [8]. The diaphysis mostly consists of a thick cortical bone surrounding the medullar cavity which is filled with bone marrow.

The inorganic phase of the bone is made of Hydroxyapatite mineral crystals. These are reported to have low crystallinity and high surface to bulk ratio. It is a calcium deficient apatite with chemical formula $Ca_{10}(PO_4)_6(OH)_2$). The crystals are plate shaped with dimensions of 2 – 6 nm thick, 30 – 50 nm wide and 60 – 100 nm long. These crystallites are reported to be the smallest biologically formed crystals. The mineral crystals are embedded in the organic matrix and provide the mechanical strength required [4] [5].

The organic phase of bone is predominantly made of Type I collagen which is the most abundant fibril forming protein in the body. Type I collagen molecule has a fibrous nature and each fibril is made of three polypeptide chains, each chain consisting of more than 1000 amino acids. These polypeptide chains forms into a triple helix structure with right handed symmetry. The amino acids present in polypeptide chains follow Glycine – X – Y sequence where X and Y are more frequently represented by proline and hydroxyproline [4]. The organic phase plays an important role in providing the flexibility to the bone structure. Non – Collagenous proteins (NCPs) are also present in the organic phase but are usually less than 10% of total proteins. They play an important role in bone mineralization. The other major component in bone is water which plays an important role in improving the overall toughness of organic and inorganic interface [5].

2. HEIRARCHIAL ORGANIZATION OF BONE

The structure of bone has different hierarchical levels with collagen molecules, hydroxyapatite crystals and water forming the basic elements. The basic collagen molecule is called as Tropocollagen which has triple helix structure of three polypeptide chains. Tropocollagen units are 300 nm in length, 1.5 nm wide and are have the long axis parallel to the fibril. They are arranged in quarter – staggered array leading to a formation of periodic banding pattern called as D – band. The D – band has a length of 67 nm which is characterized by 40 nm gap region and 27 nm overlap region. A bundle of the tropocollagen units form a collagen fibril and the collagen matrix forms a scaffold for mineralization.

The mineralization that takes place within a collagen fibril is called as intrafibrillar mineralization which starts from the gap regions present due to arrangement of tropocollagen units. The minerals grow as platelets of HAP along the long axis of fibril. As the mineralization increases, they continue to grow and occupy the overlap regions as well. Eventually the crystals join together by compressing the tropocollagen units and form extended sheets. Apart from the mineralization observed within the collagen fibril, large amount of mineralization is also present between collagen fibrils and this type of mineralization is called extrafibrillar mineralization which accounts for 75% of total mineral content. The gaps between collagen fibrils also consist of large number of non-collagenous proteins. The crystals observed in extrafibriallar mineralization are reported to be thicker than intrafibrillar mineralization but have the same plate like structure [4].

The composite of collagen fiber and HAP forms a strong and stiff structure and it has been reported that collagen fibril has a soft core covered by a hard shell [5]. A mineralized collagen fibril is the basic structural unit for bone tissue and a bundle of collagen fibrils forms into collagen fiber. These mineralized collagen fibrils are organized into various patterns of fibril arrays resulting in different mechanical properties. These fibril arrays are selected or fine-tuned to match different

functionalities of the bone. Woven array has small bundles of mineralized collagen fibrils randomly organized and is the weak form of bone. Parallel fibril arrays are developed when the fibrils are arranged parallel to the long axis of the bone. The other important type of fibril array is lamellar formation which is made of several parallel fibril arrays. Each layer of lamellae has varying thickness and orientation of collagen fibrils [2] [4]. At microscopic level both cortical and spongy bone are made of lamellae that are laid flat and curved around in circles. But the center of lamella in cortical bone is formed into osteons to protect the haversian canals which consist of blood vessels and nerve tissues.

3. BONE REMODELLING

There are two types of bone formation. During the initial stages of bone formation, a spurt of bone modelling takes place adding new bone mass and developing the size, shape of bone. Over a period of time the total volume of bone settles down and bone remodeling takes place. As the bone remodels itself the old or damaged bone is replaced with new bone material. At a given repair site no additional bone mass is added and the new bone mass created will be similar to the bone mass removed. Bone remodeling helps the bone to fine-tune and repair itself to withstand loads and remove any micro-cracks accumulation [3].

There are different types of bone cells responsible for bone remodeling like Osteoblasts, Osteoclasts, Osteocytes and Bone lining cells [8]. All these cells are located in the bone marrow and are recruited to repair sites through various small channels. Since trabecular bone has more surface contact with bone marrow which consists of all bone cells, it undergoes large amount of bone remodeling compared to cortical bone. It has been reported that about 25% of spongy bone is remodeled every year while only 3% of cortical bone is remodeled for the same time. This implies that spongy bone of patients affected by osteoporosis is heavily affected [9]. Osteoclasts are responsible for bone removal and originate from hematopoietic cell lineage. These cells have

a ruffled border underneath, which increases the surface interface between the cell and the bone surface. It also acts a seal between the osteoclast and bone surface of repair site. This zone is called sealing zone [1]. Osteoclasts then release acids in the sealing zone which dissolves the mineral content of the bone matrix in repair site. Once the mineral content is dissolved, osteoclasts then excrete enzymes which remove the remaining collagenous matrix. Due to this resorption pits are formed along the exposed bone surface. This entire process is called bone resorption [10].

Bone remodeling is a coupled process and as the osteoclasts preform bone resorption they release cytokines which signal osteoblast recruitment. Osteoblasts originate from osteoprogenitor cells and are also called as bone formation cells. The progenitor cells are biological cells that have an ability to differentiate into specialized cell types and these cells are usually present in the bone marrow. Osteoblasts fill in the resorption pits and lays down organic matrix called Osteoid which is predominantly Collagen. This forms a scaffold for crystallization of minerals like calcium and phosphate [11]. As the resorption pit is filled with new bone material some of the osteoblasts convert into bone lining cells and cover the surface of the bone. Bone lining cells are flattened and inactive osteoblast cells and can undergo differentiation into osteoblasts back and forth. They are believed to be sensitive for mechanical stimulation, osteoclasts released chemicals during resorption and osteocyte signals.

Some active osteoblasts are trapped in the matrix they secrete and become Osteocytes. Osteocytes develop long processes which radiate about 15 μm in every direction. These cells are interlinked with the help of small channels called as canaliculli which have around 200nm radius and form a complex network in bone [12]. These cells are responsible for intercellular signaling and bone communication and are highly sensitive to mechanical loads. These cells can sense any increased work load on bone and respond by triggering differentiation activity of osteoblasts to increase bone density and thereby decreasing the stress points. When bone undergoes constant under loading for prolonged durations, osteocytes communicate with osteoclasts to increase resorption and remodeling to eliminate under loaded bone. Loss of bone mass decreases the overall strength and

increases the risk of fracture. This highlights the importance of staying fit and maintaining good nutritional diet [13].

There are several models to explain the process of bone mineralization. Most of these models underline the importance of collagen structure. Although collagen is an important component in bone mineralization, it needs the help of non-collagenous proteins to initiate oriented mineralization process [5]. The non – collagenous proteins have large number of acidic amino acids. The acidic amino acids determine the binding capacity of NCPs to polyvalent metal ions like calcium which plays an important role in mineralization process. Some of the NCPs bind to specific locations on triple helices based on molecular recognition mechanisms. They can control the crystal size and shape, inhibit mineralization and also stabilize transient mineral phases. A single non – collagenous protein is found to effect mineralization in several different ways. It was observed that proteins in solution at high concentration can inhibit mineralization while at low concentration can influence the size of the mineral particles [4].

Bone mineralization is a complicated process and there are several hypotheses to explain the driving force behind it. ACP theory proposed the existence of amorphous nature to mineral particles during initial stages of mineralization [14]. Other reports indicate formation of inorganic substance in bands filling the gaps in collagen molecules and then transforming into needle like structures [15]. Recent report has contradicted these models and proposed the presence of liquid – phase amorphous precursor for mineral particles which gets drawn into gaps of collagen molecules due to capillary forces. Once driven into gaps of collagen molecules, they start to solidify and crystalize thereby forming nanoscopic hydroxyapatite crystals embedded in the collagen matrix [4].

4. WOLFF'S LAW

Wolff's law explains the adaptability of bone matrix to mechanical stresses. A recent review article discussed the relevance of piezoelectricity and other mechanisms [16]. The charge distribution and potential generated due to mechanical stresses is denoted by the term SGP (Stress Generated Potential). The most researched mechanisms for explaining SGP are piezoelectricity and streaming potential. Piezoelectricity is believed to play an important role in SGP for a dry bone whereas as for wet bone streaming potential is believed to play a major role. It has to been reported that calcium hydroxyapatite plays an important role in dehydrating bone tissue by blocking access of water to collagen [17] [18]. The stress generated potential can be expressed in terms of mathematical equations for both piezoelectricity and streaming potential [16].

For piezoelectricity, $V = (d_{ijk}L/\varepsilon)B\exp(-\sigma t/\varepsilon)$

Where d_{ijk} – third rank piezoelectric tensor; L – sample thickness; σ – load applied to the sample and t – time.

For Streaming potential, $V = (\zeta\varepsilon\Delta P) / \sigma\eta$

Where: ζ – zeta potential; ε – dielectric permittivity; ΔP – pressure gradient; σ – solution conductivity and η – solution viscosity.

The basis of streaming potential theory lies in the studies on canaliculli which play a mechano – sensory role by providing channels for osteocytes to sense fluid shear forces. The in – vitro studies need much higher strains than in-vivo studies to induce cellular response in bone cells. Canalicular fluid flow hypothesis is been put forth to address this discrepancy. According to this theory canaliculli and lacunae function as pressure transducers. The fluid in these channels flow towards harversian canal through thin layer of non-mineralized matrix and cell processes. This fluid flow in turn activates the cell surface glycocalyx and initiates biochemical process for osteogenisis. It has also been reported that the fluid flow and in-vivo strain increased the levels of intracellular

Ca^{+2} and protein kinase which simulates factors responsible for bone growth. The surface charge density can influence streaming potential and properties of bone. The chain of events start with compression of collagen fiber which results increase in surface charge density generating higher zeta potential. This is followed by an increase in streaming potential, electro osmosis and reduction in hydraulic permeability. As a result the dynamic stiffness of tissue is increased. From the above chain of events it is evident streaming potential can directly modify bone tissue stiffness. Piezoelectricity can change the surface charges upon mechanical stress thereby indirectly influence both zeta potential and streaming potential in compression. This leads to influencing the stiffness and fluid dynamics of bone tissue [16].

Although streaming potential mechanism has been strongly favored recently, it does not explain any mechanism which can help osteocytes to differentiate between different types of stresses. With the lack such mechanism for recognizing different stresses, streaming potentials cannot be solely responsible behind the complex microarchitecture of bone which is carefully designed to sustain different types of stress [19]. It is believed that piezoelectricity of collagen plays an important role in sending signals to osteocytes based on types of stresses because of its orientation and anisotropic properties. This lends support to the idea that both piezoelectricity and streaming potential can work together for bone formation rather than either one of them being solely responsible.

5. PIEZOELECTRIC PROPERTIES OF BONE

Recent developments in surface imaging have resulted in developing a new technique called as Piezoelectric Force Microscopy (PFM). PFM is a scanning probe microscopy technique similar to Atomic Force Microscopy (AFM) but is based on the reverse piezoelectric effect for imaging the samples. Piezoelectricity is an electromechanical property where application of mechanical stress can induce surface charge density for some materials. The reorganization of electric dipole moments at nanometer scale results in the piezoelectric properties in materials. PFM uses AFM

tips that are coated with conductive material to improve the electrical contact between sample and tip. Periodic bias voltage is applied to the tip and the resultant mechanical strain is measured from deflection of cantilever. If the initial electrical domain of the sample is perpendicular to surface and parallel to applied field, the domain expand bending the cantilever upwards. If the domains are anti – parallel to the applied field, the domains contracts resulting in decreased cantilever deflection [20]. PFM has been used to image individual collagen fibers on fascia tissue which are rich in type I collagen at nanoscale resolution. Collagen fiber bundles with 2 – 10μm wide and D – band (67nm) have been observed in the PFM images. The report also finds that the PR originating from overlap regions in collagen fibrils have stronger signal than gap regions which has been attributed to the C_6 symmetry of fibrils in overlap regions [21].

Studies performed on demineralized rabbit bone samples demonstrated the effect of collagen piezoelectricity on mineralization. A biomimetic system is developed to simulate in vivo conditions. Bone samples are demineralized by dissolving them in 0.5 M EDTA at pH 7.4 and the resultant collagen substrates are placed in a plastic tube. Due to the shape of the plastic tube the substrates undergo sufficient stress to separate collagen molecules and generation piezoelectricity. A simulated body fluid (SBF) is prepared to simulate body fluid and is maintained at body temperature and pH. The fluid is circulated throughout the column and collagen substrates are exposed to the fluid through a window. After performing the experiment for three weeks the substrates showed change in mineral composition to the control sample. The compressed side of collagen substrates underwent more mineral particle deposition compared to uncompressed (tension) side. The dipoles reorganization upon the mechanical deformation develops negative charges in the compression region. The positive charged calcium ions present in SBF are attracted to the negatively charged compression region which nucleates and crystalizes to hydroxyapatite (HA). The experiments also indicated depletion of hydroxyapatite on the tension side of collagen substrates. The positive polarity developed on tension side is put forth as possible explanation for depletion of hydroxyapatite. The report further argues that bone mineralization can also be a purely electrochemical deposition. Another hypothesis is that the change in surface energy and charge distribution when hydroxyapatite crystals are formed could act as signal for osteoblast and osteoclasts recruitment [22].

6. MECHANICAL BEHAVOIUR OF BONE

The mechanical behavior of bone tissue at different levels varies according to its hierarchical levels and its composition. The organic phase is straightjacketed between mineral plates which adds stiffness to the organic and inorganic composite. The spaces between collagen fibers are filled by mineral crystals which establish an intermolecular chemical interaction and are mediated by non – collagenous proteins. These mineralized collagen fibrils form parallel array arrangement and runs along the longitudinal axis of the bone. The micro indentation studies on bovine femur revealed difference in hardness values between longitudinal and transverse planes. The highest hardness values are observed along transverse plane and lowest in longitudinal face – on plane while the longitudinal edge – on plane has intermediate hardness value. The hardness values are heavily influenced by the position of mineral particles in the composite matrix [4].

Another load distribution model argues that the stiff mineral particles withstand tensile forces while the collagen fibrils slide against each other. Mineral particles and non – collagen proteins form viscoelastic medium filling the gap regions in collagen fibrils. It has been noted that the interfibrillar shear is higher than the forces observed in collagen fibrils and mineral particles. This indicates an increase in stiffness from nanoscale to mesoscale [23]. The non – collagenous proteins forms supramolecular networks which dissipate huge amounts of energy under mechanical load. They act as glue between collagen fibers, improving fracture resistance and contributing to overall strength and toughness [24].

Osteons play an important role in fracture resistance. Osteon number increases with age often leading to direct contact between neighboring osteons. Bone forms ark – shaped micro cracks in every lamella under compressive load. These micro cracks radiate outwards from the center and play an important role in absorbing a part of the load. They also help in deflecting the crack propagation and preventing failure at significantly high loads [3].

Bone remodeling depends on a synchronous effort from different factors and precursors. When this fine balance is disturbed by various reasons, it results in diseases such as Osteoporosis, Osteopetrosis, and Osteoarthritis etc. Osteoporosis which is a most prevalent disease with more than 200 million estimated affected people around the world. It is caused due to increased activity of osteoclasts over osteoblasts. Several reports have been published explaining the causes and possible treatments for this disease. Osteopenia is a bone disorder known as a precursor for osteoporosis where the bone mineral density is reported to be below than normal. According to World Health Organization (WHO) the bone mineral density for a osteoporosis affected bone is about 2.5 standard deviation below mean peak bone mass of a healthy bone. It is more commonly observed in elder women after menopause. Due to the decreased bone mineral density the affected bones have high risk of bone fracture [25].

7. OBJECTIVE

The overall objective of this thesis is to observe changes in chemical composition and micro – structure as a result of bone aging and osteoporosis. Healthy and osteoporotic rat femur bone samples of two age groups are collected for material characterization. Atomic Force Microscope is used to observe the changes in topography for young and old rat femur bones. It is also used to observe changes in microstructure between healthy and osteoporotic samples. The changes in chemical composition and elemental distribution are observed using a High Resolution Scanning Electron Microscope (HRSEM). It is also used for high resolution imaging of bone samples.

8. Materials and Methods:

8.1. Sample Preparation:

Bone samples of Sprague – Dawley rats are collected from Dr. Stefan Judax research group of BME Stony Brook University which are categorized into healthy and osteoporotic with age control. The rats are divided into two groups at age of 5 months and one set of these rats are overiectomized (OVX) and the other group is of healthy rats (AC). One group of AC and OVX rats are sacrificed at age of 6 months. The next group of AC and OVX rats is sacrificed at 12 months age group. The left femoral diaphysis is extracted and cleaned of the soft tissue. The samples are then preserved in ethanol solutions (70%, 80%, 90%, and 100% for 3-4 days) at -20°C. After the samples are dehydrated, they are embedded in epoxy resin with proximal end exposed. The surface of the samples are polished using abrasive silicon carbide papers of decreasing particle size (600, 800 and 1200) and were then polished with a series of diamond suspension solution (3μm, 1μm, 0.025μm and 0.05μm). The blocks are then cross sectioned parallel to the long axis of the bone. The face of the block has perpendicular cross-section of spongy bone with cortical bone acting as boundaries. The samples are divided into 4 groups based on age and medical condition. They are labelled as 6AM, 6OVX, 12AM and 12OVX. The number denotes the number of months for bone sample, AM for healthy bone and OVX for osteoporotic bone samples [26].

8.2. Atomic Force Microscopy

A Vecco MultiProbe Scanning Probe Microscope is used for AFM imaging to observe topographical changes. Since the AFM sample holder cannot accommodate epoxy resin bone blocks due to size restrictions, they are sectioned into thin slices with approximately 20μm thickness using Microtome equipment. These thin slices are then transferred onto small pieces of

Silicon wafer which can fit into the sample holder of the AFM. The specifications of the AFM tips used are shown in Table 1 and 2.

Table 1: Specifications of AFM tip

Maker	Burker
Model	TESP
Material	0.01 – 0.025 Ohm – cm Antimony (n) doped Si

Table 2: Specifications of AFM tip cantilever

T	3.25 – 4.75μm
L	110 – 140μm
W	30 – 50μm
K	20 – 80 N/m
f_0	294 – 387 kHz

AFM tool is operated in tapping mode since the samples are very delicate and contact mode can damage the samples. Scan – Dual mode is selected and the Height and Phase channels are used for scanning. The scan rate is maintained at 0.3 Hz to obtain better resolution and the scan sizes varied between 1μm to 5μm. The amplitude setpoint and drive amplitude parameters are optimized to obtain a high resolution AFM scan image. The AFM imaging is performed on 5 different locations (1, 2, 3, 4 and 5) on each sample. These locations are chosen to acquire an average of results and observe any possible trends across the surface of the specimens. The figure 1 shows the selected regions on a bone sample.

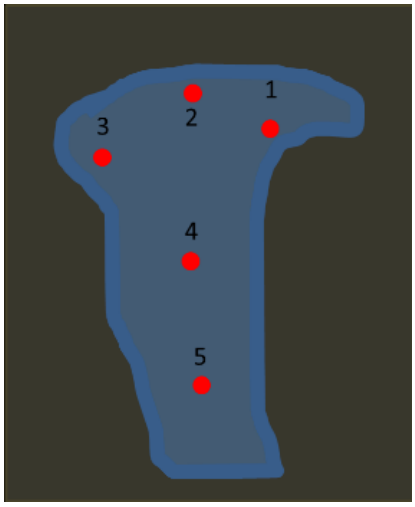

Figure 1: Representive image of AFM datapoints (1, 2, 3, 4 and 5) on bone sample.

8.3. Scanning Electron Microscope

A JEOL7600F High Resolution Analytical SEM (HRSEM) is used for high resolution imaging and chemical analysis of the samples. Since the samples are embedded in non – conductive epoxy resin blocks, it causes charging effect when placed in SEM vacuum chamber. When a non – conductive sample is placed in SEM vacuum chamber, the negative charge of the electrons doesn't transmit to ground through sample holder. This forms charged atmosphere near surface of the sample thereby distracting the subsequent incoming electrons and degrading the scan image quality. The samples are hence coated with carbon using a Gatan Model681 High Resolution Ion Beam Coater to reduce the charging effect. The parameters are optimized to produce a carbon coating of 1µm thickness on the specimen. This improves the conductivity leading to decrease in charging effect and better image quality. The epoxy resin block is further covered with a double sided carbon tape apart from the visible bone area to further decrease any chance of charging effect and improve the image quality.

9. Results

9.1. Atomic Force Microscope analysis

The samples from healthy and osteoporotic groups of different age groups are characterized using Atomic Force Microscope. The height and phase images obtained for these groups are presented in the figures 2, 3, 4 and 5.

A.

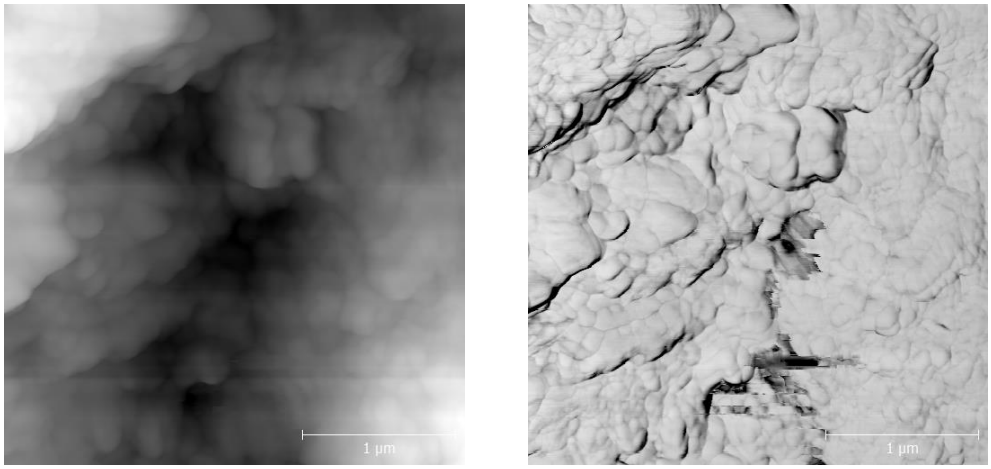

B.

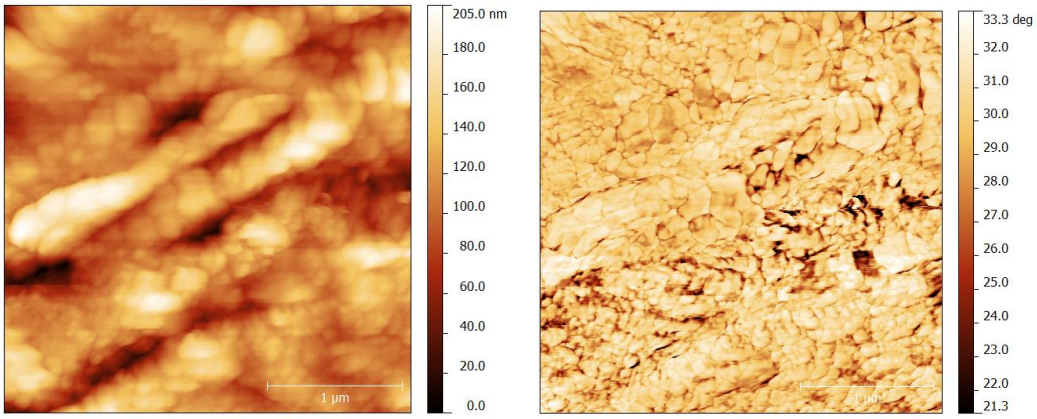

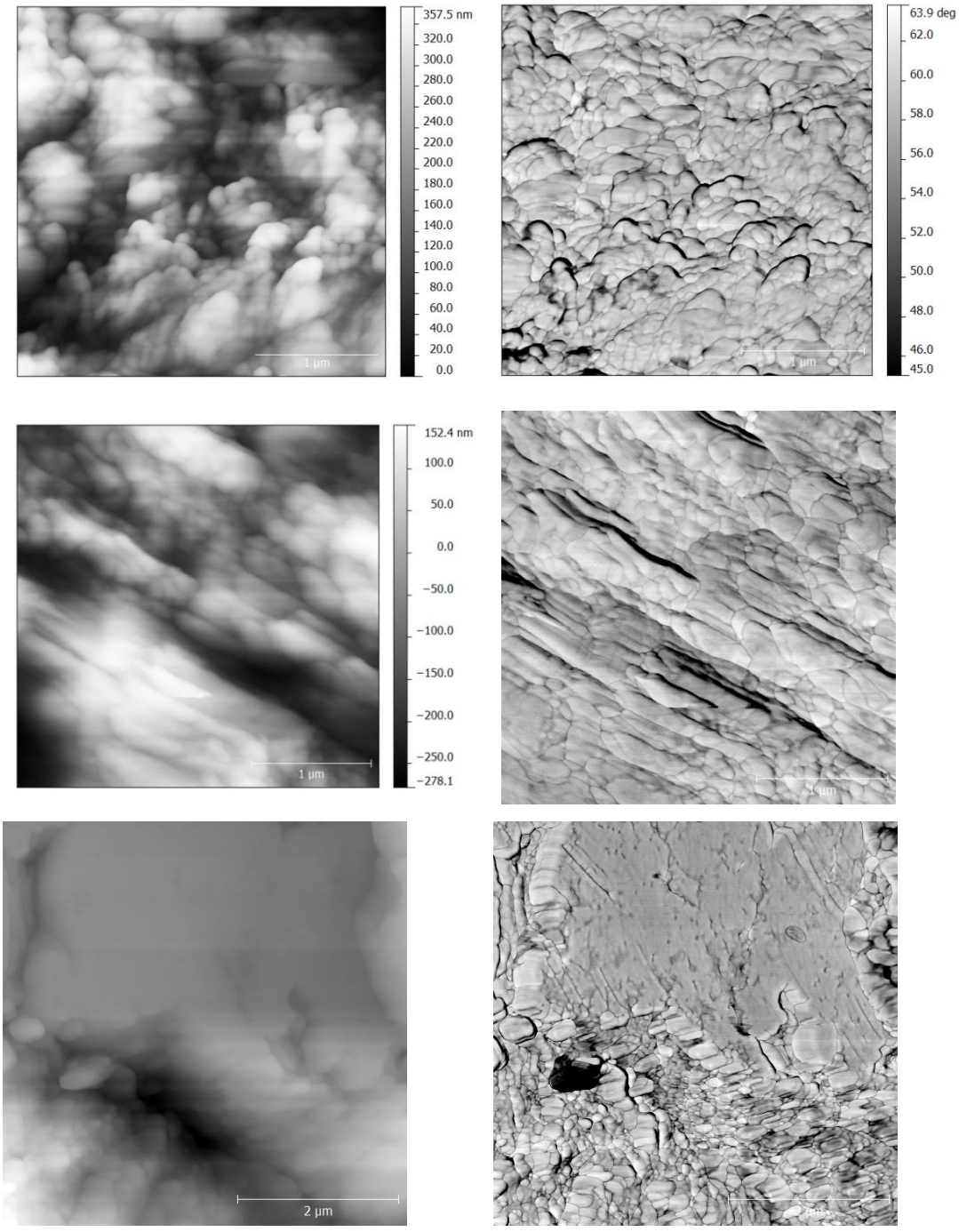

Figure 2: AFM scan Height and Phase images of 6AM sample: A) Height and Scan images on data point 1, B) Height and Scan images on data point 2, C) Height and Scan images on data point 3, D) Height and Scan images on data point 4, E) Height and Scan images on data point 5.

A.

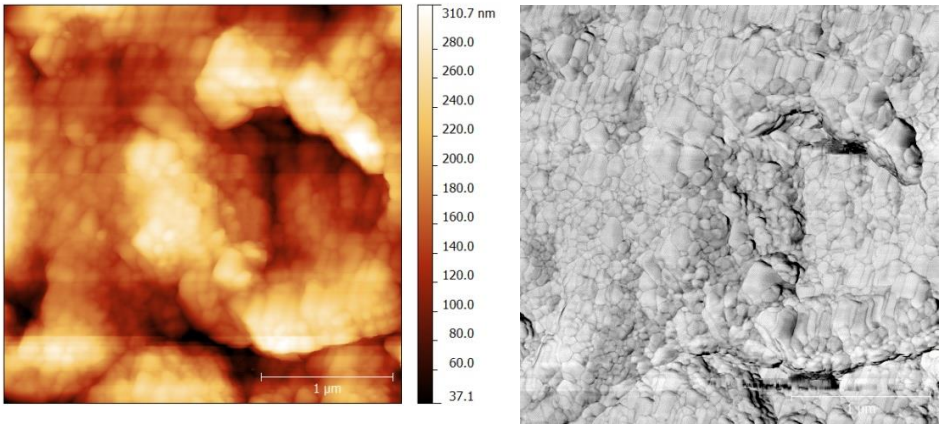
310.7 nm
280.0
260.0
240.0
220.0
200.0
180.0
160.0
140.0
120.0
100.0
80.0
60.0
37.1
1 µm

B.

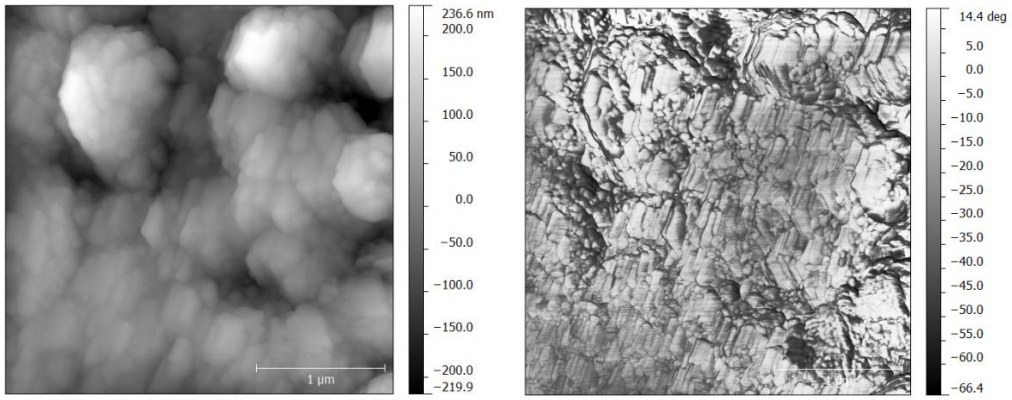
236.6 nm
200.0
150.0
100.0
50.0
0.0
−50.0
−100.0
−150.0
−200.0
−219.9
1 µm
14.4 deg
5.0
0.0
−5.0
−10.0
−15.0
−20.0
−25.0
−30.0
−35.0
−40.0
−45.0
−50.0
−55.0
−60.0
−66.4

C.

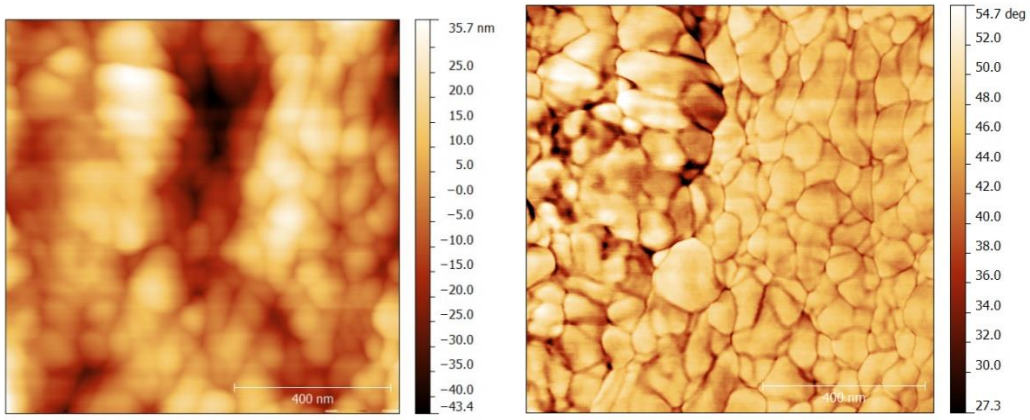
35.7 nm
25.0
20.0
15.0
10.0
5.0
−0.0
−5.0
−10.0
−15.0
−20.0
−25.0
−30.0
−35.0
−40.0
−43.4
400 nm
54.7 deg
52.0
50.0
48.0
46.0
44.0
42.0
40.0
38.0
36.0
34.0
32.0
30.0
27.3

D.

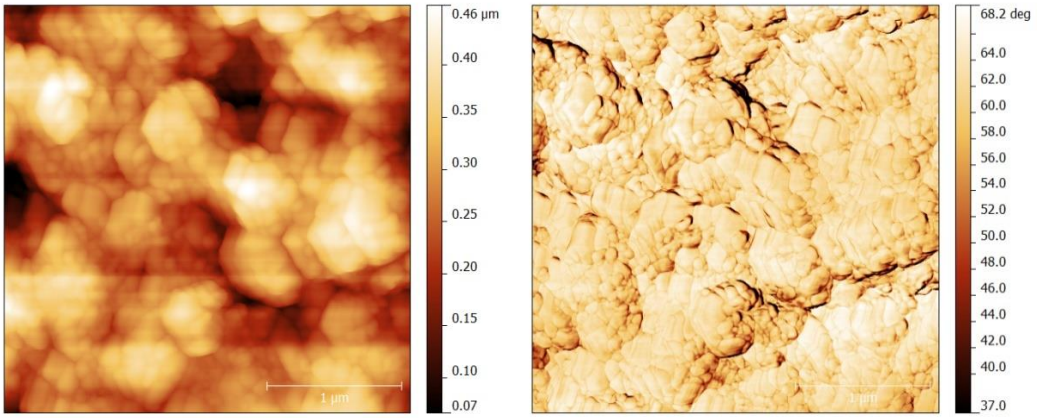

E.

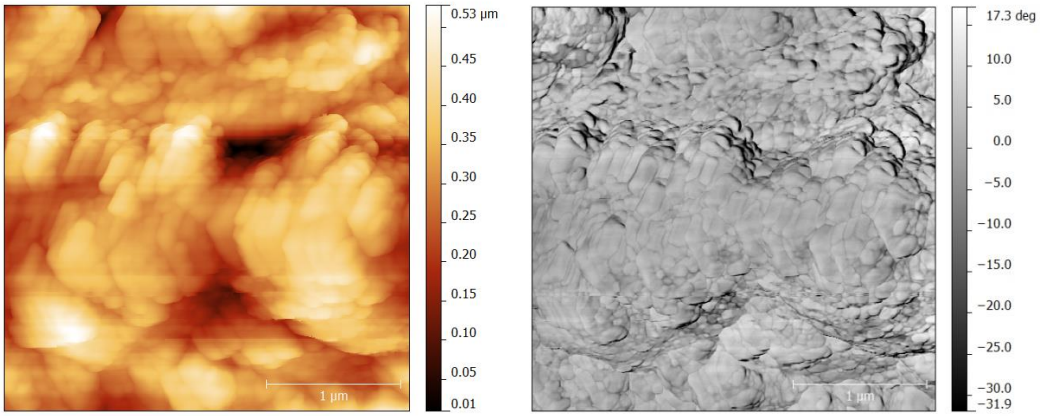

Figure 3: AFM scan Height and Phase images of 6OVX sample: A) Height and Scan images on data point 1, B) Height and Scan images on data point 2, C) Height and Scan images on data point 3, D) Height and Scan images on data point 4, E) Height and Scan images on data point 5.

A.

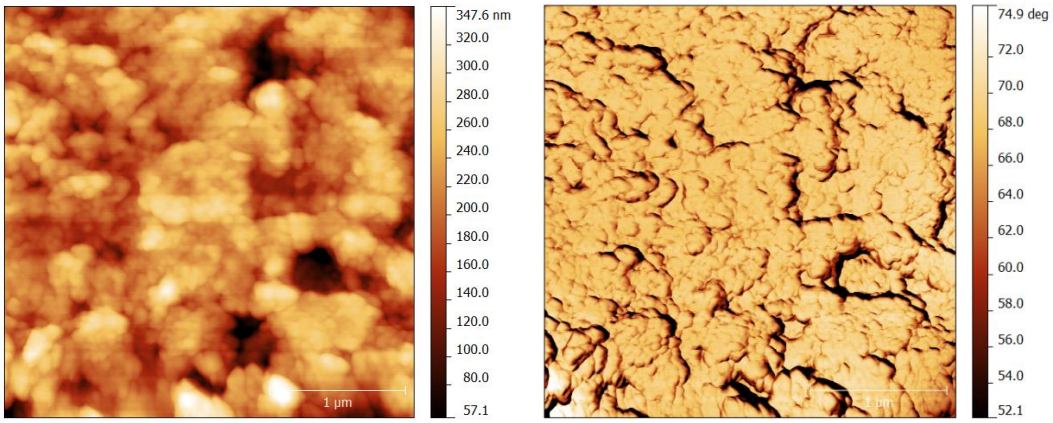
347.6 nm
320.0
300.0
280.0
260.0
240.0
220.0
200.0
180.0
160.0
140.0
120.0
100.0
80.0
57.1
1 µm
74.9 deg
72.0
70.0
68.0
66.0
64.0
62.0
60.0
58.0
56.0
54.0
52.1
1 µm

B.

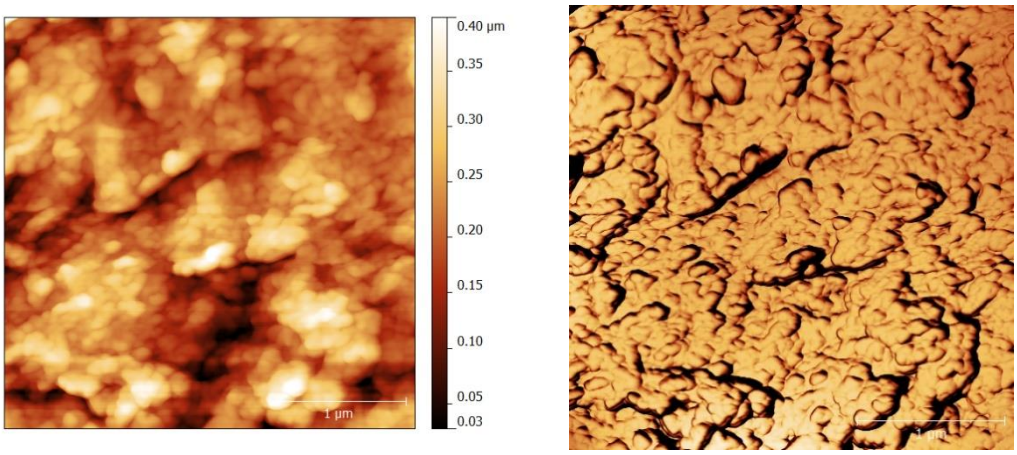
0.40 µm
0.35
0.30
0.25
0.20
0.15
0.10
0.05
0.03
1 µm

C.

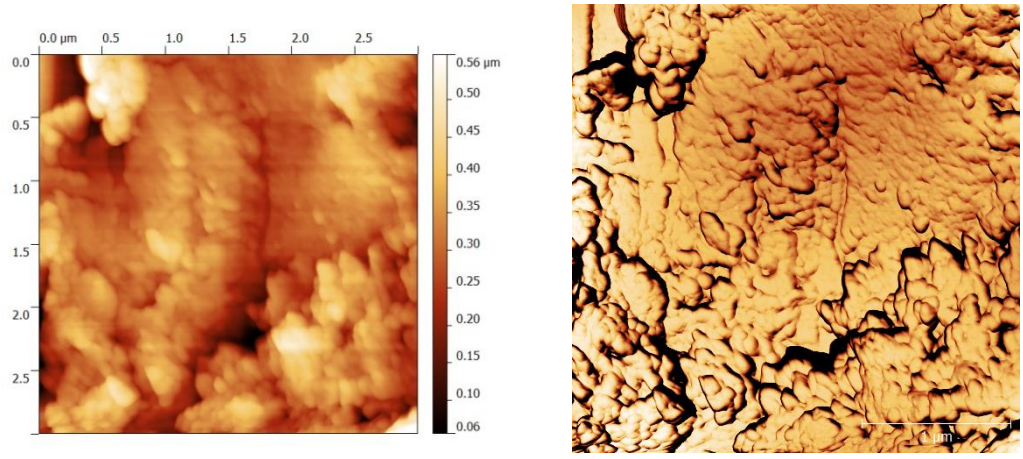
0.0 µm
0.5
1.0
1.5
2.0
2.5
0.0
0.5
1.0
1.5
2.0
2.5
0.56 µm
0.50
0.45
0.40
0.35
0.30
0.25
0.20
0.15
0.10
0.06
1 µm

D.

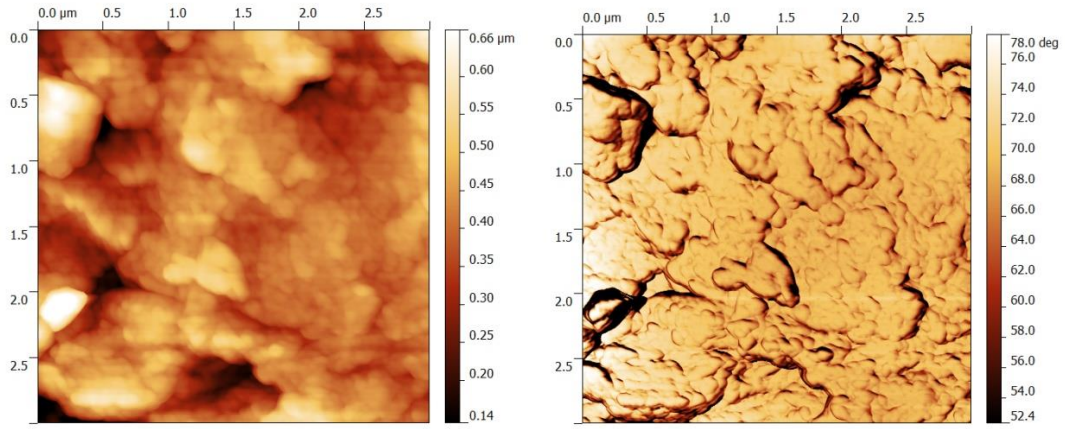

E.

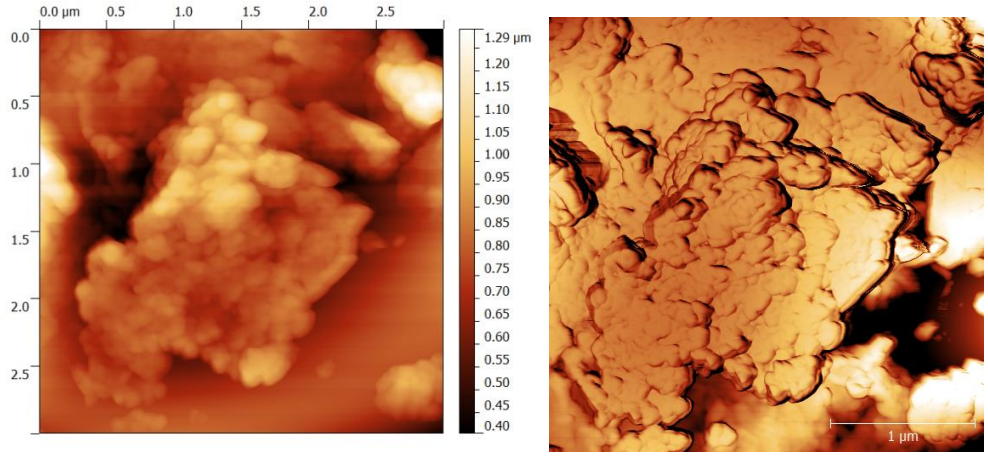

Figure 4: AFM scan Height and Phase images of 12AM sample: A) Height and Scan images on data point 1, B) Height and Scan images on data point 2, C) Height and Scan images on data point 3, D) Height and Scan images on data point 4, E) Height and Scan images on data point 5.

A.

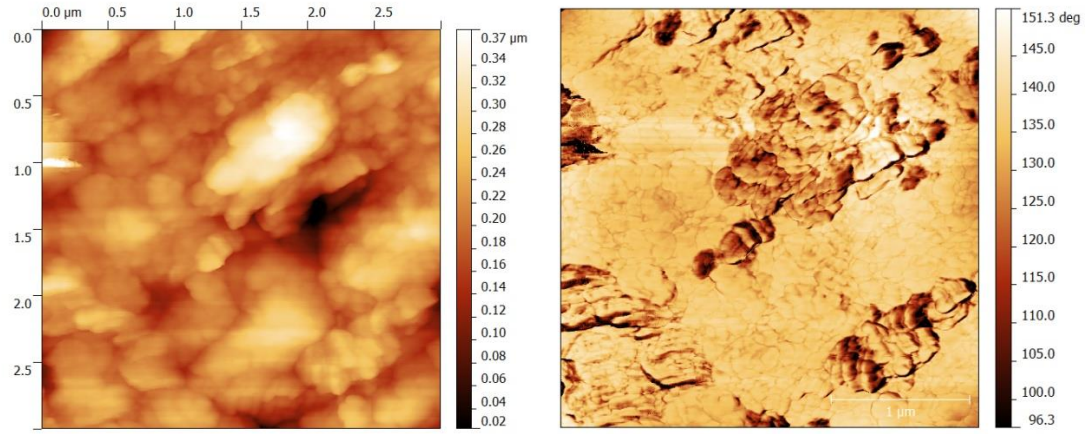
0.0 µm 0.5 1.0 1.5 2.0 2.5
0.0
0.5
1.0
1.5
2.0
2.5
0.37 µm
0.34
0.32
0.30
0.28
0.26
0.24
0.22
0.20
0.18
0.16
0.14
0.12
0.10
0.08
0.06
0.04
0.02
1 µm
151.3 deg
145.0
140.0
135.0
130.0
125.0
120.0
115.0
110.0
105.0
100.0
96.3

B.

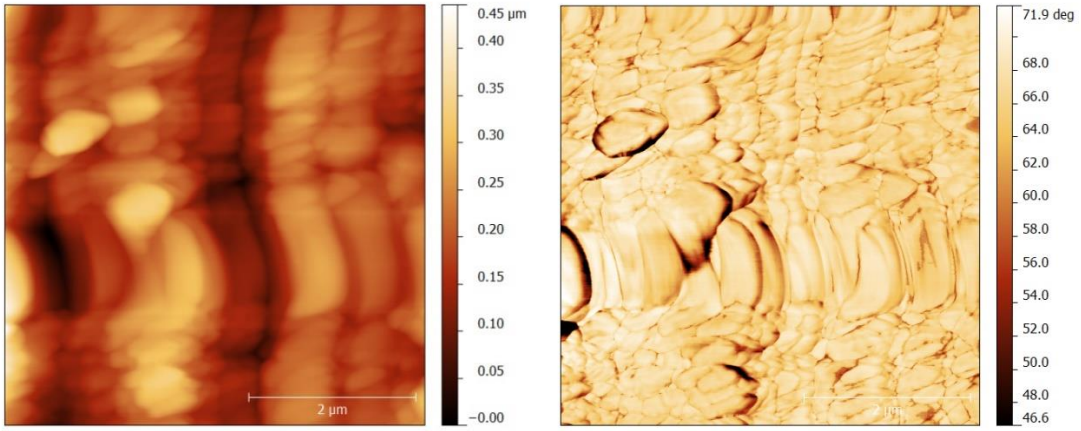
0.45 µm
0.40
0.35
0.30
0.25
0.20
0.15
0.10
0.05
−0.00
2 µm
71.9 deg
68.0
66.0
64.0
62.0
60.0
58.0
56.0
54.0
52.0
50.0
48.0
46.6

C.

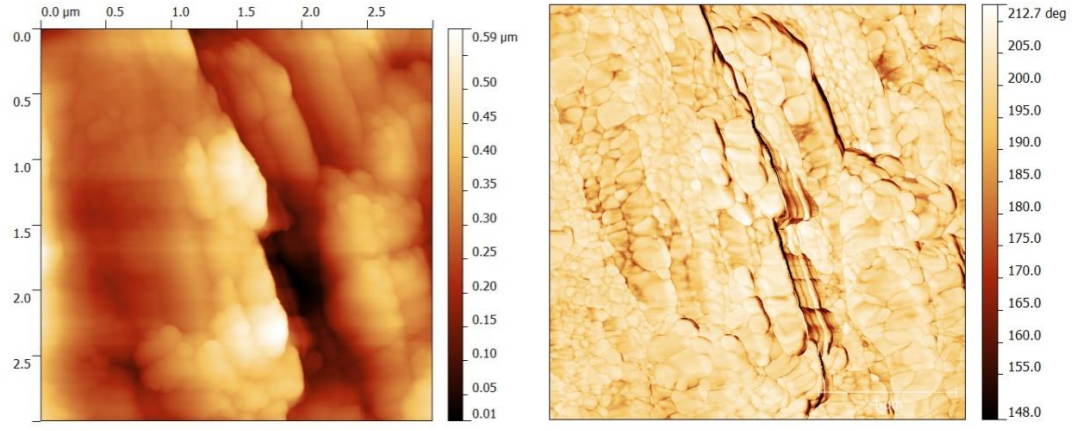
0.0 µm 0.5 1.0 1.5 2.0 2.5
0.0
0.5
1.0
1.5
2.0
2.5
0.59 µm
0.50
0.45
0.40
0.35
0.30
0.25
0.20
0.15
0.10
0.05
0.01
212.7 deg
205.0
200.0
195.0
190.0
185.0
180.0
175.0
170.0
165.0
160.0
155.0
148.0

D.

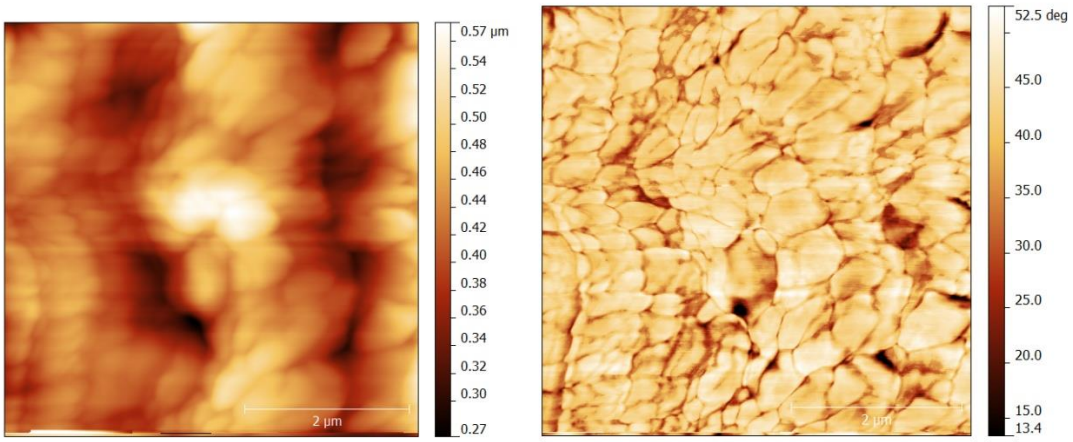

E.

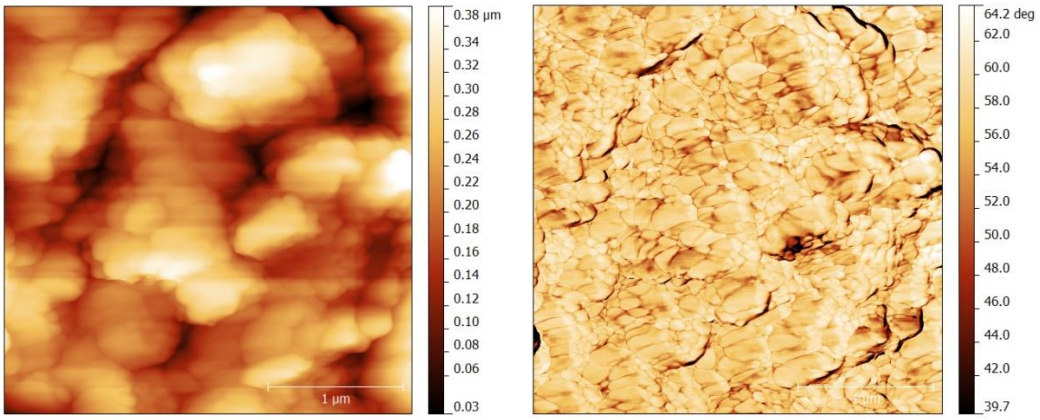

Figure 5: AFM scan Height and Phase images of 12OVX sample: A) Height and Scan images on data point 1, B) Height and Scan images on data point 2, C) Height and Scan images on data point 3, D) Height and Scan images on data point 4, E) Height and Scan images on data point 5.

9.2 Scanning Electron Microscope analysis

The samples from the four groups are scanned in low magnification at 5kV operating voltage. Scans are performed on top, middle and bottom parts of the samples to cover the entire length of the specimen. The scanned images are stitched together to form an image which represents the entire length of the sample and are shown in figure 6.

A. 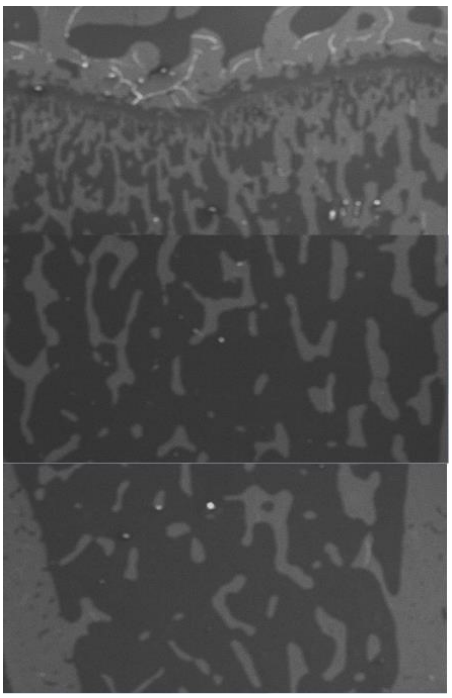 B. 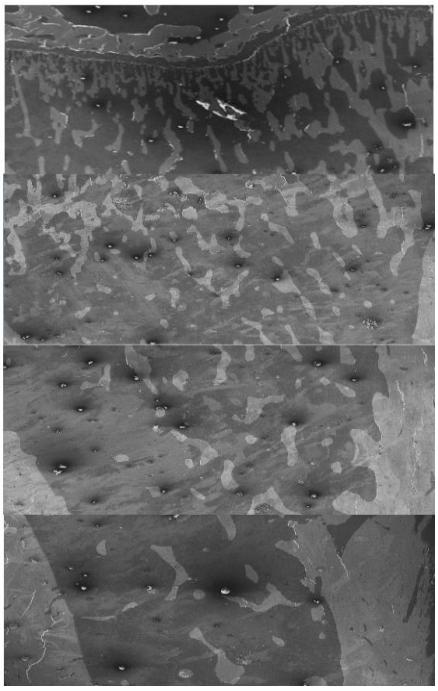

C. 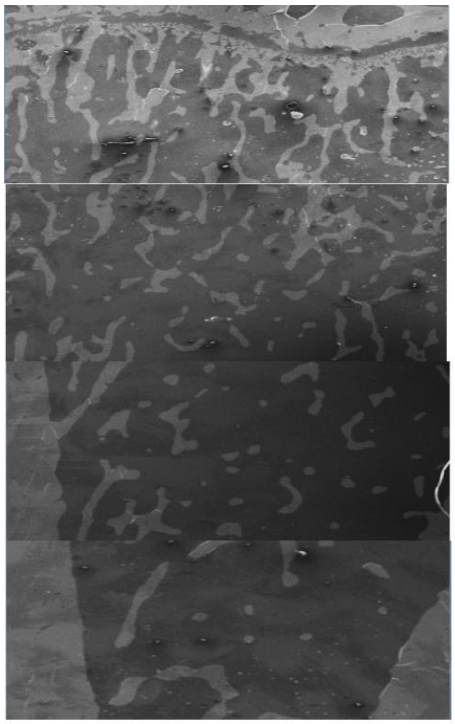 D. 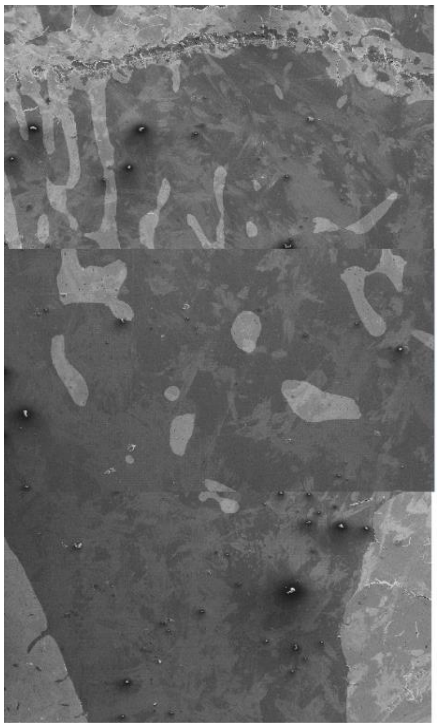

Figure 6: Scanning Electron micrograph of different samples at low magnification (45X) and 5.0 kV operating voltage. The top, middle and bottom scan images are stitched together to present overview of the sample. A) 6AM B) 6OVX C) 12AM D) 12OVX

The Quant mapping mode is used to analyze elemental distribution on samples from the four groups. The quant mapping provides images with color coding representation of energy values radiated out from the sample with red representing minimum energy and blue maximum energy at 8keV. The images acquired are stitched together to obtain an overview of the entire sample as shown in figure 7.

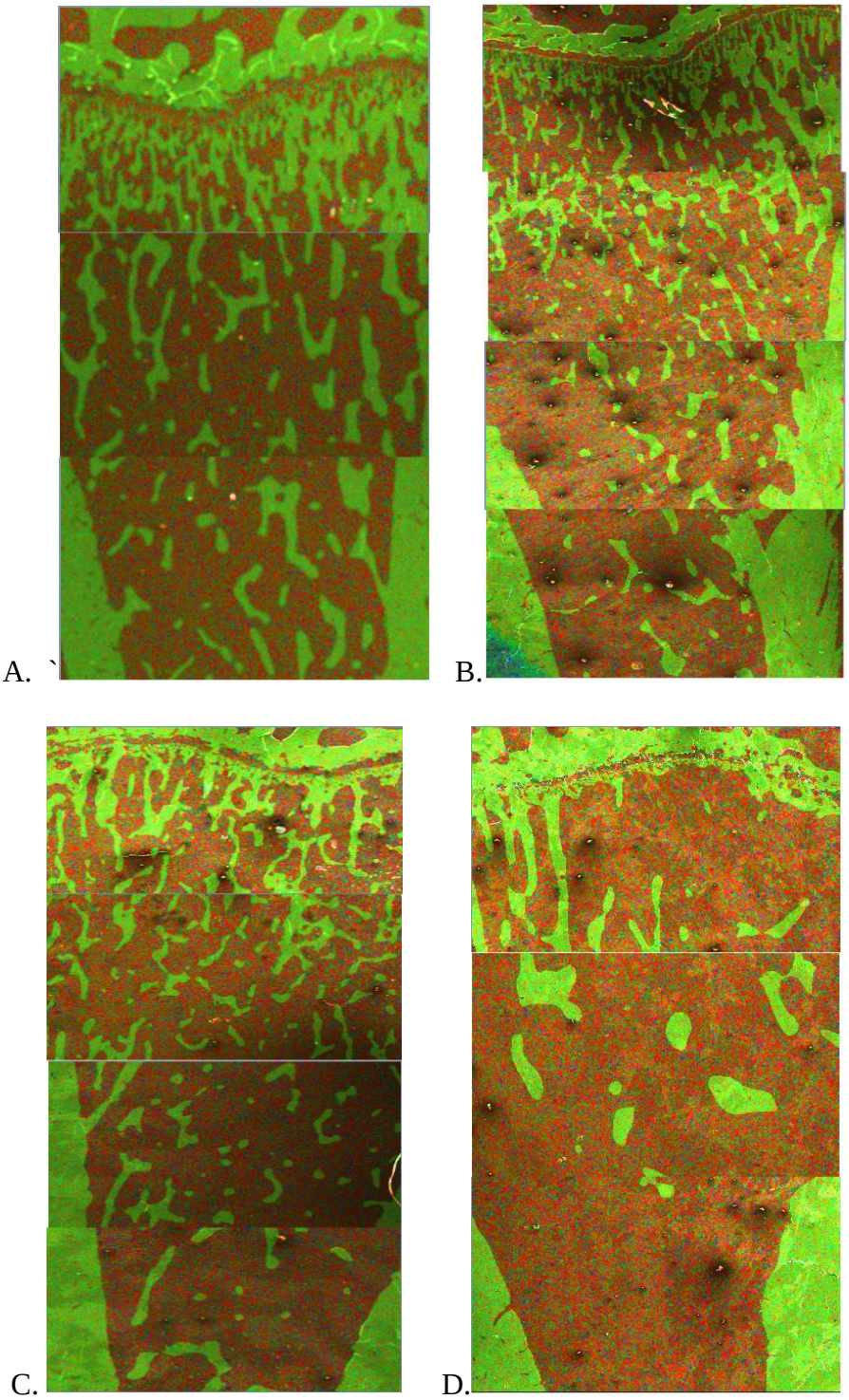

Figure 7: Quant mapping mode in Scanning Electron Microscope of different samples at low magnification (45X) and 5.0 kV operating voltage. The top, middle and bottom scan images are stitched together to present overview of the sample. A) 6AM B) 6OVX C) 12AM D) 12OVX

The samples are imaged using Gentle Beam feature available in JEOL7600F High Resolution Analytical SEM (HRSEM) for high magnification imaging. Gentle Beam feature operates at 1keV and is preferred over higher voltages to avoid burning of sample at higher magnifications. The lower operating voltage also provides better topographical information than higher voltages. The working distance for these imaging to set to 4.5 mm to achieve the resolution required at higher magnification. The pictures acquired through high resolution imaging are shown in figures 8 and 9.

A. 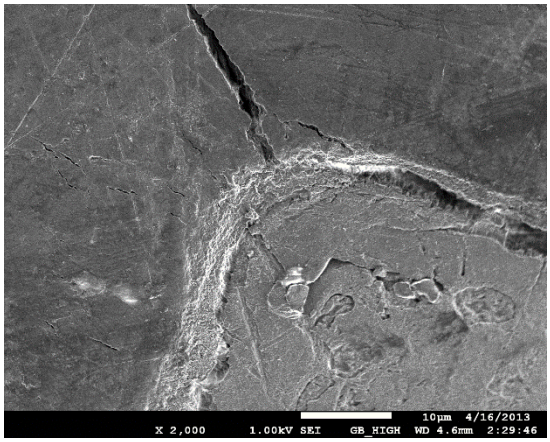

B. 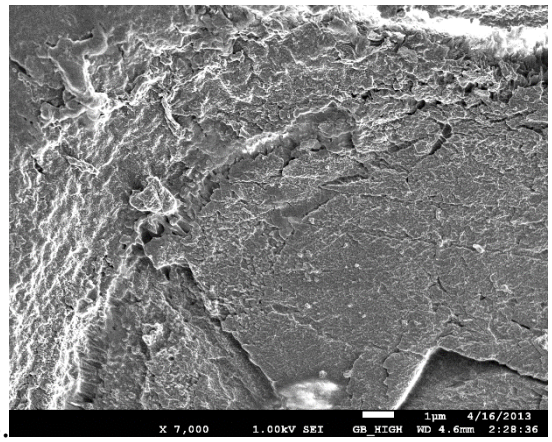

C. 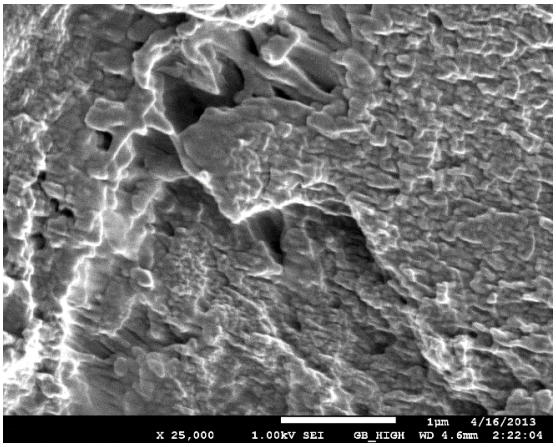

D. 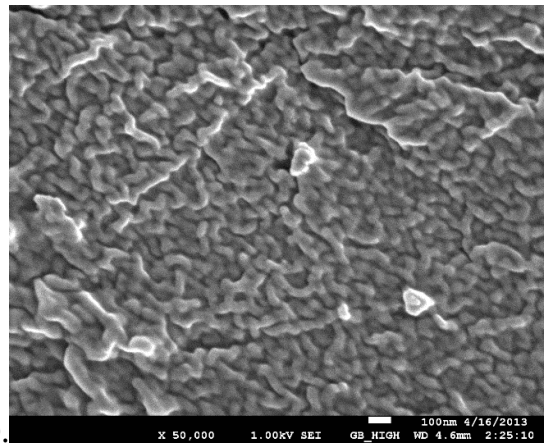

Figure 8: Gentle Beam Scanning Electron micrograph of 6OVX sample (organic phase) at high magnification operated at 1.0 kV and 4.5mm working distance A) X 2000 magnification B) X 7000 magnification C) X 25000 magnification D) X 50000 magnification

A. 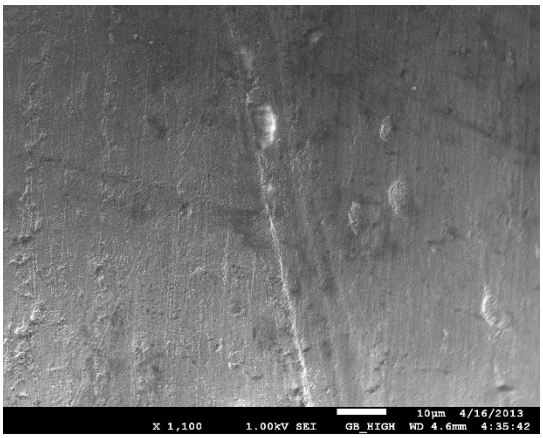

B. 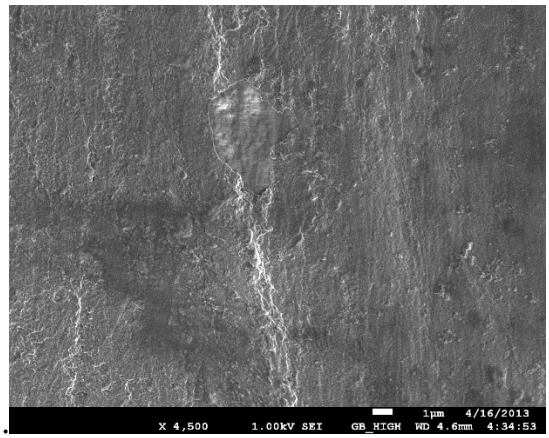

C. 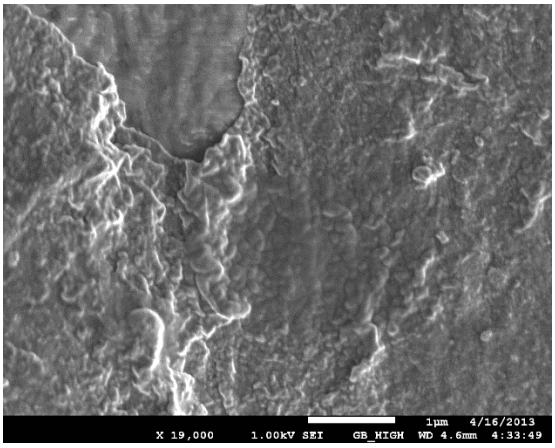

D. 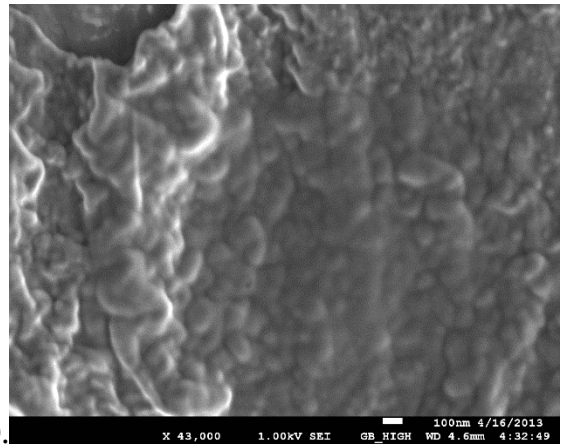

Figure 9: Gentle Beam Scanning Electron micrograph of 12OVX sample (inorganic phase) at high magnification operated at 1.0 kV and 4.5mm working distance A) X 1100 magnification B) X 4500 magnification C) X 19000 magnification D) X 43000 magnification

The samples are also characterized for elemental composition or weight percentages using Energy – dispersive X-ray spectroscopy technique. The analysis is carried out on five different regions in high magnification, it has to be noted that the regions used for EDS analysis are similar to the data points used for AFM analysis. These results are statistically analyzed using JMP software for trends and averages across different sample groups.

10. DISCUSSION

The AFM height and phase images clearly indicate the presence of regularly arranged grains – spheres. Similar grains – spheres have been observed by different authors while performing AFM studies on bone samples of human and rat bones. The variation in brightness of the AFM height images represents the topographical depth on the surface of the samples with respect to cantilever position. The valleys are represented by dark regions and peaks by bright regions on the sample surface. The grain boundaries are better visible in AFM phase images and hence these images are selected for conducting grains size analysis using a software tool called Gwyddion. The grain size analysis images for 6AM, 6OVX, 12AM and 12OVX are shown in figures 10, 11, 12 and 13 respectively.

A.

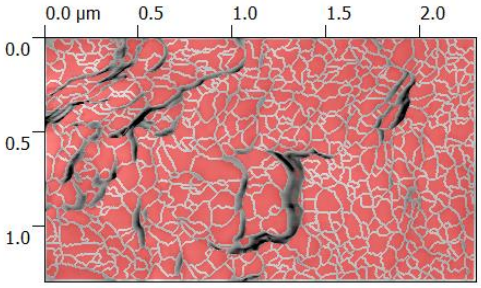

B.

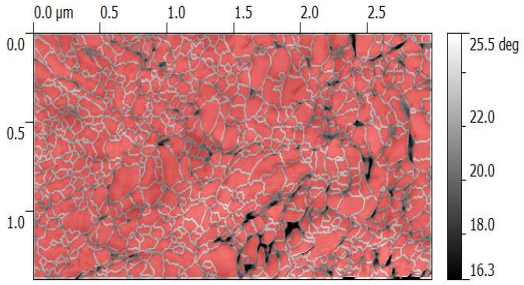

C.

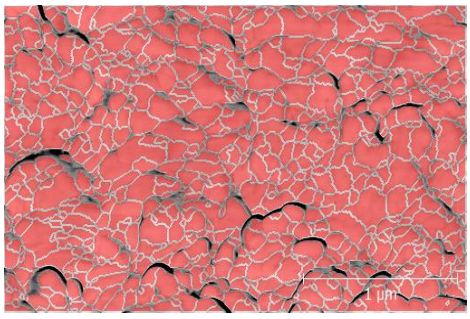

D.

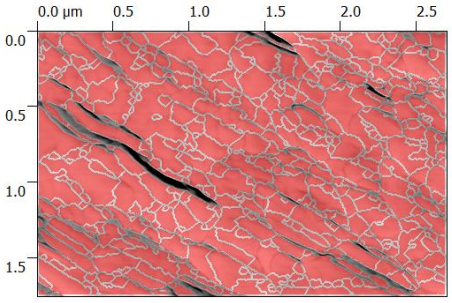

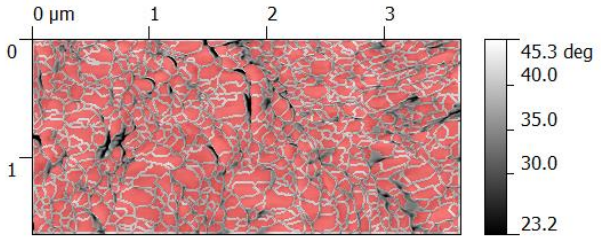

E.

Figure 10: Grain size analysis of AFM phase image for 6AM sample across data points A) First data point B) Second data point C) Third data point D) Fourth data point E) Fifth data point.

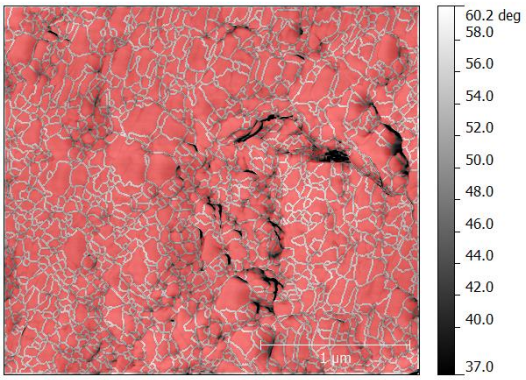

A.

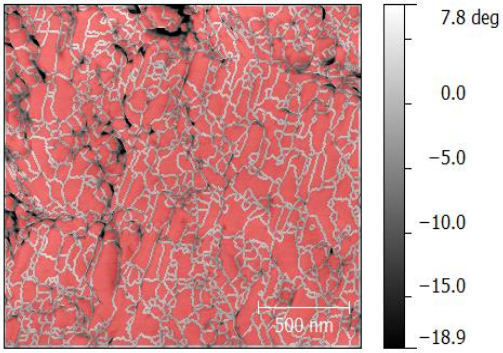

B.

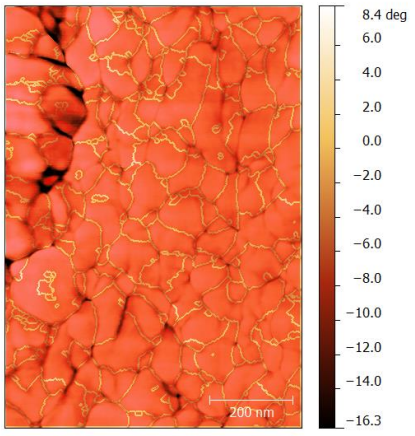

C.

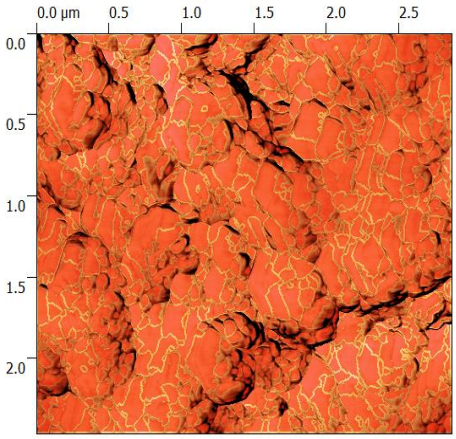

D.

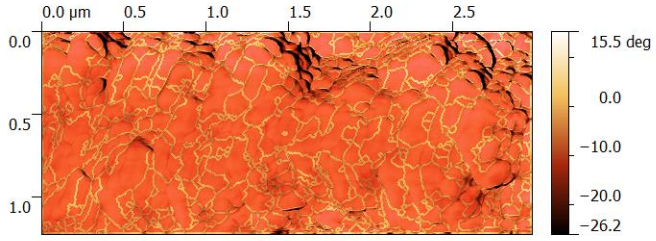

E.

Figure 11: Grain size analysis of AFM phase image for 6OVX sample across data points A) First data point B) Second data point C) Third data point D) Fourth data point E) Fifth data point.

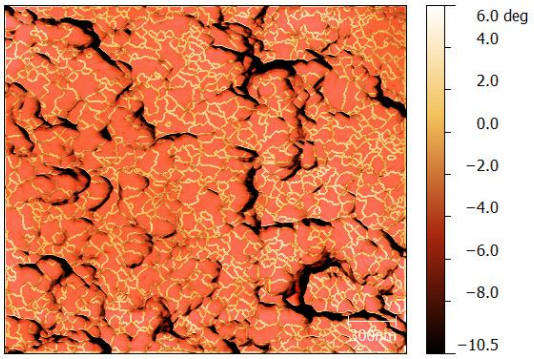

A.

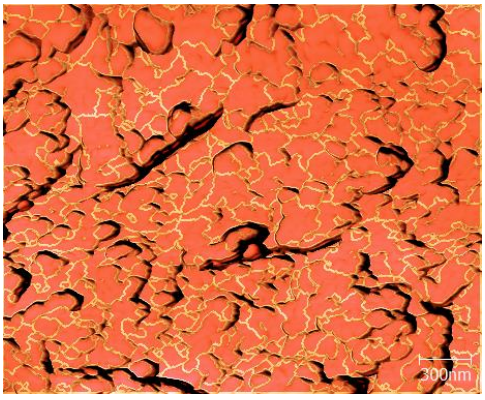

B.

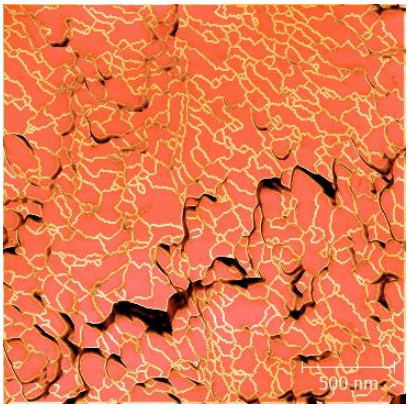

C.

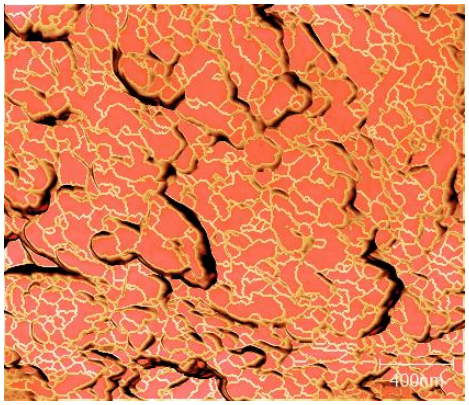

D.

E. 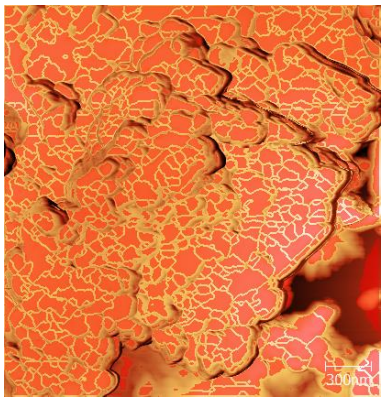

Figure 12: Grain size analysis of AFM phase image for 12AM sample across data points A) First data point B) Second data point C) Third data point D) Fourth data point E) Fifth data point.

A. 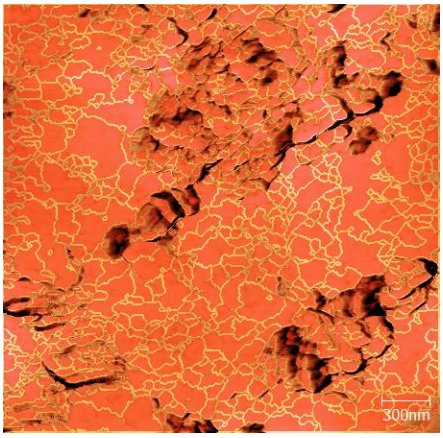

B. 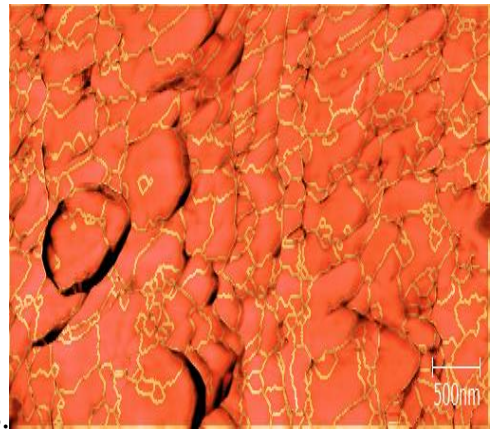

C. 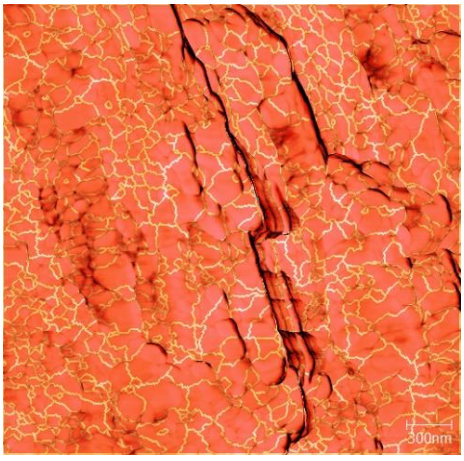

D. 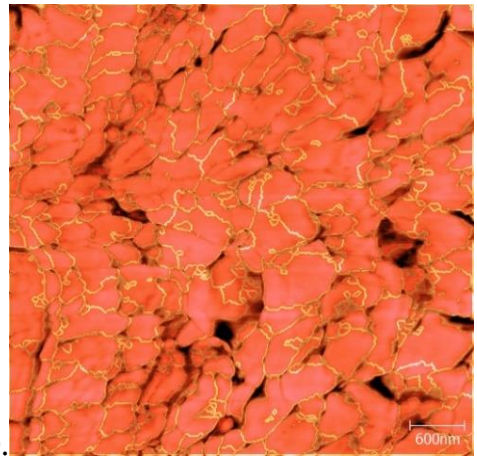

Figure 13: Grain size analysis of AFM phase image for 12OVX sample across data points A) First data point B) Second data point C) Third data point D) Fourth data point E) Fifth data point.

The grain sizes calculated using Gwyddion software and are plotted in a series of graphs to analyze the data across the different samples and locations. The graphs are shown in figures 14, 15, 16 and 17. The graphs indicate the number of grains present at a particular grain size in the samples. The X – axis is a representation of grain sphere size and Y – axis represents the number of grains.

The graphs 14 and 15 indicate the grain size distribution for 6AM and 6OVX samples. It can be observed that both these groups have high number of small grain spheres. The size ranges from 10nm – 130nm in both these groups. It can also be noted that the number of grains at particular grain size remained almost similar across the all the data points. This indicated the grain sphere size in not a function of location on the surface of the sample.

The graphs 16 and 17 show the grain size distribution for 12AM and 12OVX samples. Both these groups have higher grain sizes compared to their 6 months counterparts. The grain sizes distribution is relatively similar data points across the sample for both groups. The range of grain sizes have increased to 200nm in case of 12AM and 350nm in case of 12OVX. This is significantly higher than a maximum grain size of 130nm of 6 months samples. This indicates that the grain spheres have grown in size with age.

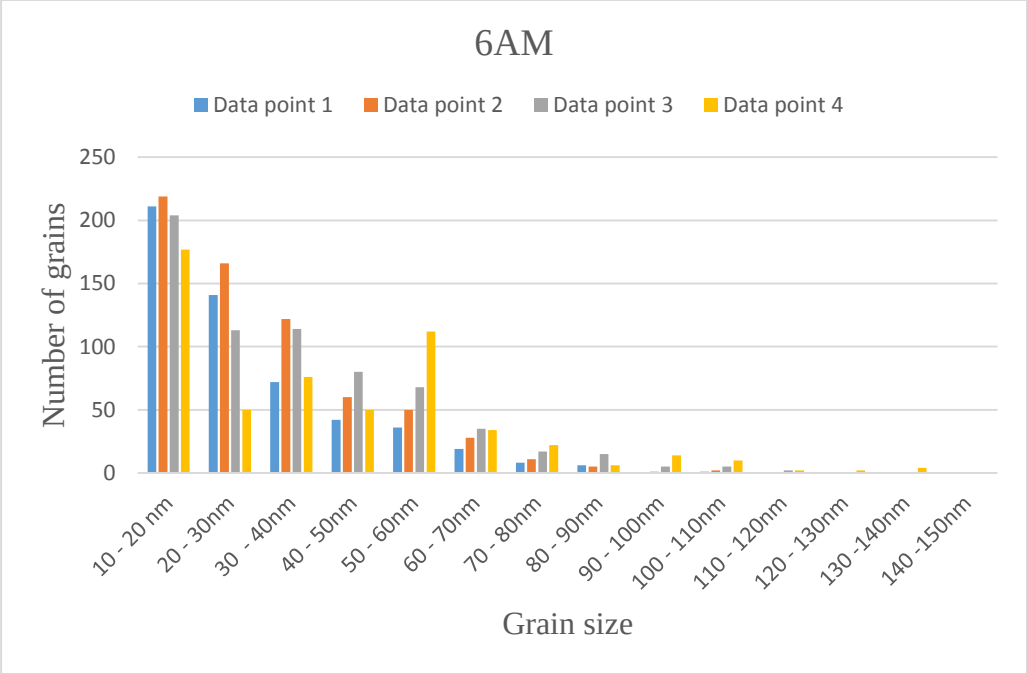

Figure 14: Graphical representation of grain size distribution between data points (1, 2, 3 and 4) for 6AM bone samples. The X – axis indicates grain size and Y – axis indicate number of grains.

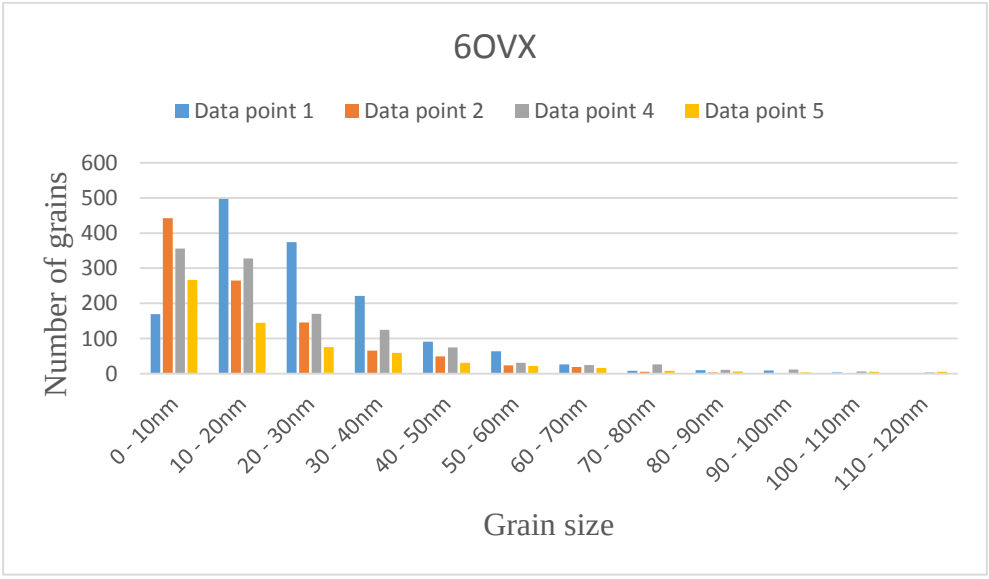

Figure 15: Graphical representation of grain size distribution between data points (1, 2, 4 and 5) for 6OVX bone samples. The X – axis indicates grain size and Y – axis indicate number of grains.

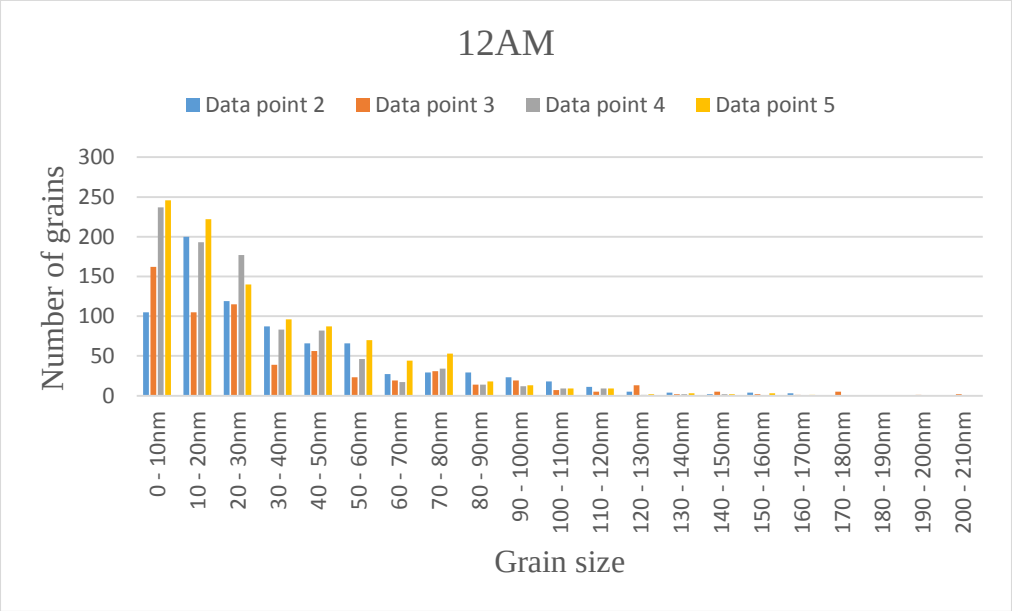

Figure 16: Graphical representation of grain size distribution between data points (2, 3, 4 and 5) for 12AM bone samples. The X – axis indicates grain size and Y – axis indicate number of grains.

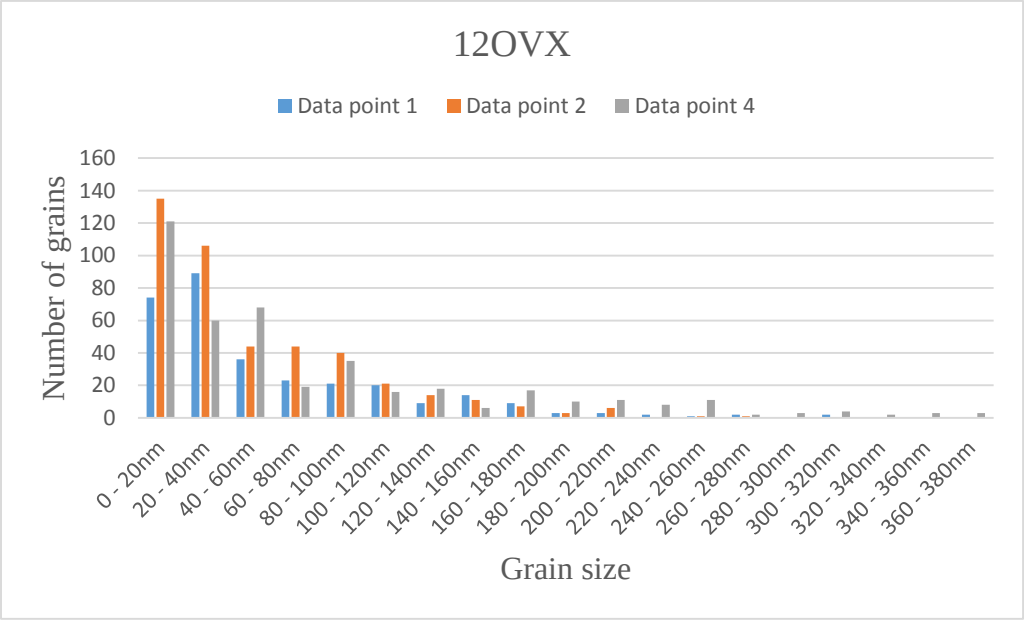

Figure 17: Graphical representation of grain size distribution between data points (1, 2, and 4) for 12OVX bone samples. The X – axis indicates grain size and Y – axis indicate number of grains.

Similar studies performed on bone samples from proximal femora of younger (20 – 40 years) and elder (73 – 94 years) women revealed an increase in mean grain size for elder samples. The grain sizes reported for younger women range between 21 – 129nm and for elder women 26 – 445nm. The elder bone samples have shown broader size distribution compared to younger samples [27]. This is similar to the grain size distribution results obtained for rat femur bone samples presented in this report. Another comparative AFM study between a healthy and osteoporotic rat femur bone also showed similar grain spheres. During this study it has been observed that the healthy bone has more regularly arranged grain spheres while the osteoporotic samples have chaotic arrangement with increased presence of amorphous HAP [28].

The figure 6 shows the low resolution SEM images for samples of different groups. The images clearly reveal the presence of a bright and darker phase. The brighter phase is seen in shape of long thin columns running through the length of the sample. It can be also observed that these columns are high in number in the top part of the sample and gradually reduce in number towards the bottom end of the samples. The 12 month group samples clearly show less number of these bright phase columns when compared to their 6 month counterpart samples.

The quant map data is further analyzed for elemental distribution of calcium, phosphorus, magnesium and sodium across the surface of the sample. The analysis has shown similar results for all the samples for different groups. The figure 18 show a low magnification scan image of top part of 6AM sample. The figures 19, 20, 21 and 22 shows the presence of calcium, phosphorus, magnesium and sodium overlaid on the 6AM low magnification scan image respectively.

The figures 19 and 20 clearly indicate that calcium and phosphorus have similar distribution across the sample. Their predominant presence in the white phase regions confirm that these regions represent the mineralized calcified regions in the spongy bone while the darker region may represent the organic matrix or bone marrow. The distribution of Magnesium and Sodium are shown in figures 21 and 22. Their distributions are similar but they don’t have any particular

pattern and can be seen almost in all areas across the sample. This can be due to the presence of nutrients both in calcified and bone marrow regions of bone.

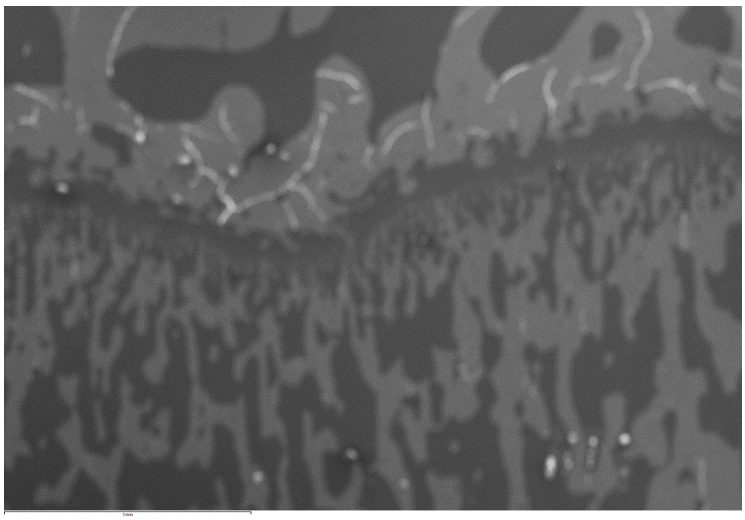

Figure 18: Scanning Electron Microscope image of 6AM top part at low magnification.

Figure 19: Scanning Electron Microscope image showing elemental distribution of Calcium as red dots overlaid on top part of 6AM sample at low magnification.

Figure 20: Scanning Electron Microscope image showing elemental distribution of Phosphorus as red dots overlaid on top part of 6AM sample at low magnification.

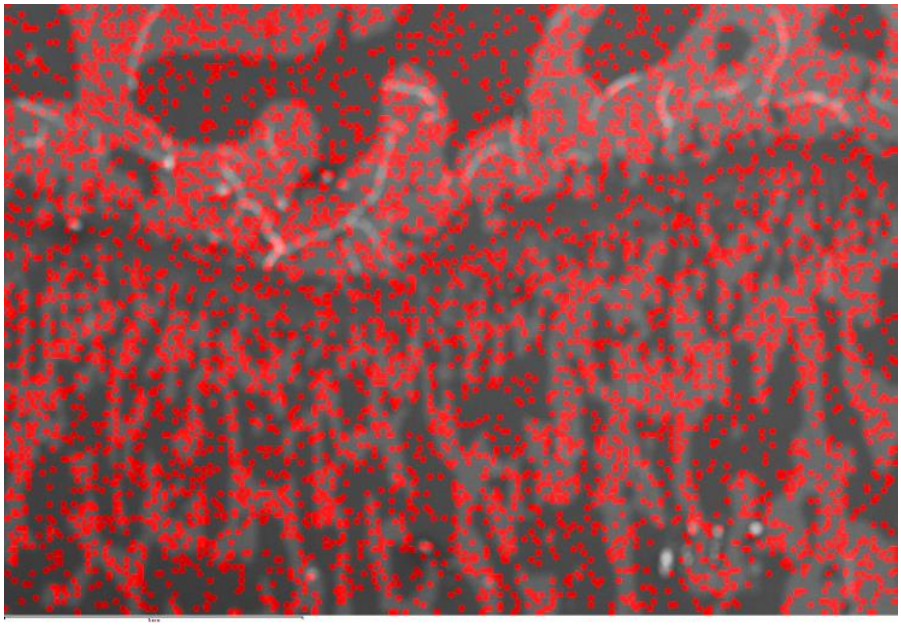

Figure 21: Scanning Electron Microscope image showing elemental distribution of Magnesium as red dots overlaid on top part of 6AM sample at low magnification.

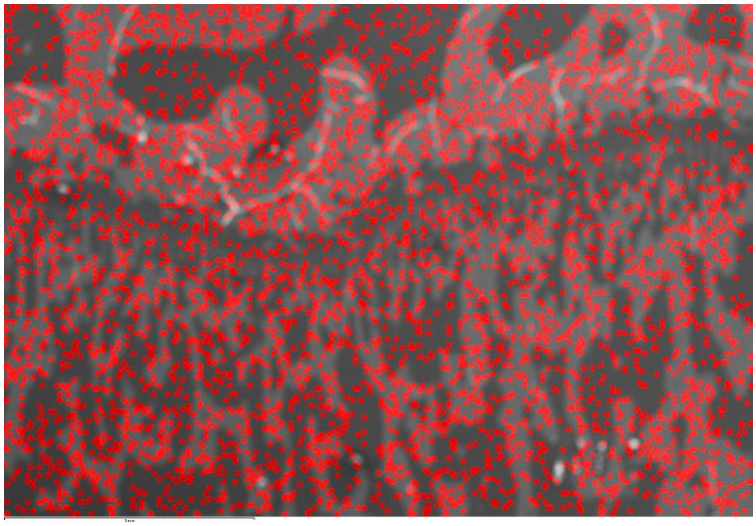

Figure 22: Scanning Electron Microscope image showing elemental distribution of Sodium as red dots overlaid on top part of 6AM sample at low magnification.

The weight percentages of various elements obtained from EDS at different locations are statically analyzed using a software tool called as JMP. The main elements observed in all the samples are calcium, phosphorus, magnesium and sodium. Hence the composition of Calcium with respect to other elements is analyzed.

The figure 23 show box plot statistical analysis performed using JMP software tool for ratio of calcium and phosphorus weight percentages across samples of different groups. The mean ratio values noted in this analysis for 6AM, 6OVX, 12AM, 12OVX samples are 1.79848, 1.79981, 1.85575 and 1.80083 respectively. Even though the 12 months age group samples recorded a slightly higher mean values than 6 months age group samples, it can be argued that the Calcium to Phosphorus ratio has remained mostly constant with respect to age of the samples. It can also be concluded that the osteoporosis did not show any impact on the calcium to phosphorus ratios. It has been reported that the calcium to phosphorus ratio did not change with age when similar analysis was performed on young and elder women bone samples [27] [29].

The box plot analysis of calcium to magnesium ratio for the different sample groups are shown in the figure 24. The mean ratio values for 6AM, 6OVX, 12AM and 12OVX are 43.9339, 45.1186, 53.2322 and 53.8716 respectively. At 6 months age group samples the OVX samples recorded a slightly higher Calcium to Magnesium mean ratio. It can also be noted that the 12 months age group samples have lot higher mean ratio values than their 6 months counterparts. At 12 months age group samples the ratio mean values are almost similar for both healthy and OVX samples.

The figure 25 shows the box plot analysis of calcium to sodium ratio values for all the sample groups. The mean value of calcium to sodium ratio for 6AM, 6OVX, 12AM and 12OVX are 52.8334, 53.949, 49.286 and 44.194 respectively. The 12 months age group samples have a slightly lower mean values compared to the 6 months age group samples. It can also be noted that across all the three ratios (Ca/P, Ca/Mg and Ca/Na), the 12 months healthy bone recorded more higher range than 6 months healthy bone.

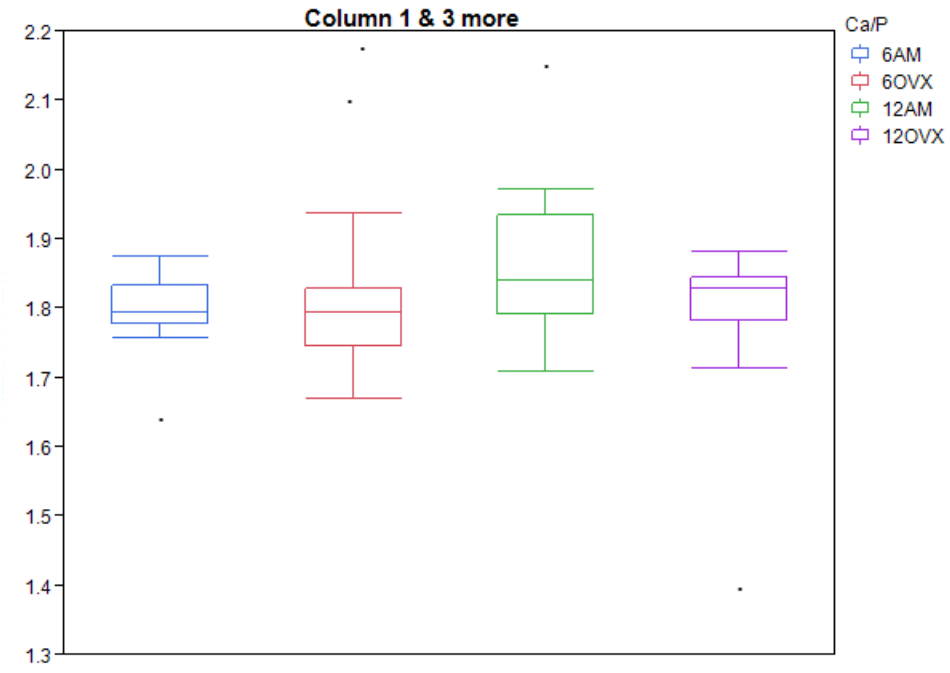

Figure 23: Box – plot analysis of calcium to phosphorus ratio across all data points among 6AM, 6OVX, 12AM and 12 OVX samples.

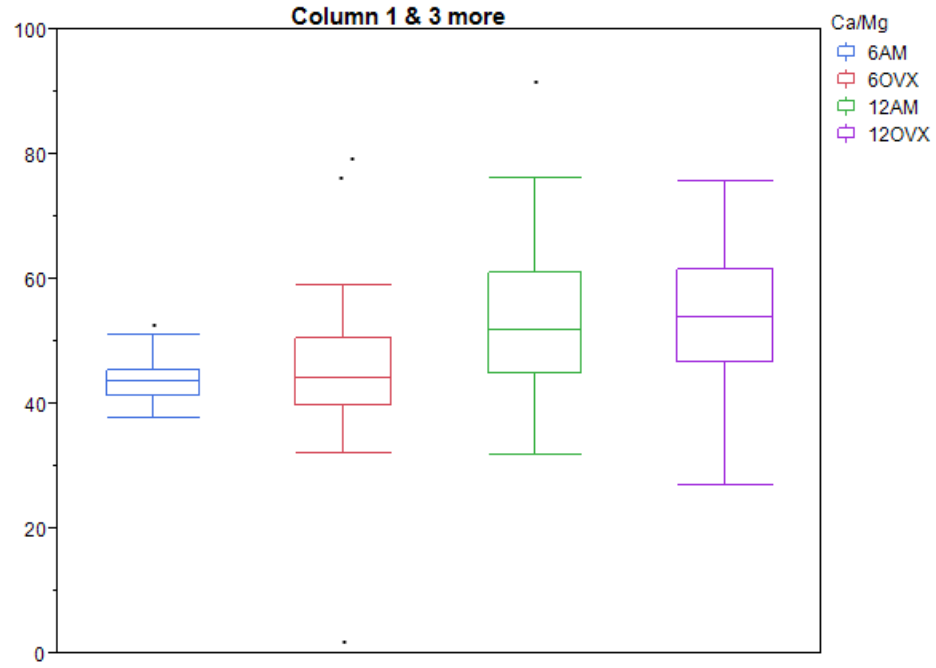

Figure 24: Box – plot analysis of calcium to magnesium ratio across all data points among 6AM, 6OVX, 12AM and 12 OVX samples.

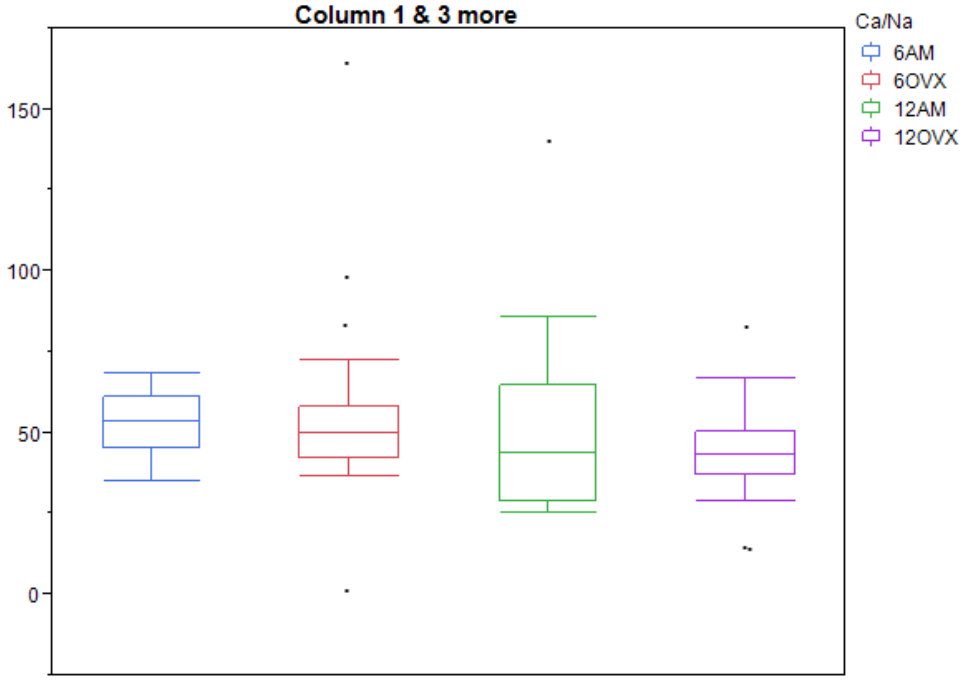

Figure 25: Box – plot analysis of calcium to sodium ratio across all data points among 6AM, 6OVX, 12AM and 12 OVX samples.

11. CONCLUSION AND SCOPE OF FUTURE WORK

The topographical analysis between young and old rat femur bone revealed that the young bones have smaller grain size distribution with higher percentage of small grains. As the bone undergoes aging the grain spheres grow in size and the grain size distribution also broadens. This suggest the grains spheres grows during aging. Since the calcium to phosphorus ratio did not vary much from younger to older bone samples in EDS analysis, the growth is grain size cannot be due to formation of new larger grains. Hence the larger grain sizes observed in older samples can be due to the aggregation of smaller grains to form a large grain. Both healthy and osteoporotic bone samples of same age group have similar grain size distribution. The decrease in mechanical strength of the osteoporotic bones can be attributed to less mineralized regions in spongy part when compared to a healthy bone. The elemental composition remained similar between healthy and osteoporotic bone samples of same age group. The calcium to magnesium ratio increased with bone aging indicating a decrease in magnesium content.

The experiments using AFM can be designed to obtain more mineral phase topography. The grain spheres observed in the AFM data can be explored and explained better. The reason behind decrease in magnesium content with aging can be explored. The samples can be tested for mechanical strength and the results can be correlated to the topographical and chemical composition data presented in the thesis.

REFERENCES

1. Loveridge, N., "Bone: more than a stick". J Anim Sci, 1999. 77 Suppl 2: p. 190 – 6.
2. S. Weiner and H.D. Wagner., "The material bone: Structure – Mechanical function relations". J Annu. Rev. Mater. Sci. 1998. 28:271 - 98
3. David Taylor, Jan G. Hazenberg and T. Clive Lee., "Living with cracks: Damage and repair in human bone". Nature materials, no.4. pp. 264 – 268, 2007.
4. Elia Beniash., "Biominerals – hierarchical nanocomposites: the example of bone". Wiley Interdiscip Rev Nanobiotechnol. 2011; 3(1): 47 – 69.
5. Mathew J. Olszta et al., "Bone Structure and formation: A new perspective". J Materials Science and Engineering R, Volume 58, issue 3 - 5 (2007), p. 77 – 116.
6. Hall, Susan. (2007) Basic Biomechanics. Fifth Edition. p.88
7. Jae – Young Rho et al., "Mechanical properties and the hierarchical structure of bone". J Medical Engineering & Physics, Volume 20, Issue 2, March 1998, p 92 – 102
8. Malaval, L; et al., "Cellular expression of bone – related proteins during in vitro osteogenesis in rat bone marrow stromal cell cultures". J Cell Physiol, 1994. 158(3): p. 555 – 72.
9. Manolagas, S.C., "Role of cytokines in bone resorption". Bone, 1995. 17(2 Suppl):p. 63S – 67S
10. Brian R. Macdonald, Maxine Gowen., "The cell biology of bone, Bailliere's Clinical Rheumatology, Volume 7, Issue 3, October 1993, Pages 421 – 443.
11. Parfitt, A.M; "Interpretation of bone densitometry measurements: disadvantages of a percentage scale and a discussion of some alternatives". J Bone Miner Res, 1990. 5(6): p. 537 – 40.
12. Bonewald, L.F. and M.L.Johnson., "Osteocytes, mechanosensing and Wnt signaling", Bone, 2008. 45(4): p.606 – 15
13. Burger, E.H. and J. Klein – Nulend. "Mechanotransduction in bone – role of the lacuna – canalicular network". Faseb J; 1999. 13(9001): p.101 – 112.
14. A.S. Posner, F. Betts, A.L. Boskey, Nc Blumenth, "Amorphous calcium phosphate – hydroxyapatite – bone mineral formation analog system, J. Bone Joint Surg.: Am. A 56(1974)860

15. E. Bonucci., “Calcification in Biological systems”, CRC Press LLC, Boca Raton, 1992, 432 pp.
16. Andrew C. Ahn et al., “Relevance of collagen piezoelectricity to “Wolff’s Law”: A critical review”. J Medical Engineering & Physics 31 (2009) 733 – 741.
17. S.A.M. Tofail., “Piezoelectricity of Bone from new Perspective”. Electrets (ISE), 2011 14th International Symposium on, vol., no., pp.91, 92, 28 – 31 Aug. 2011.
18. J.C. Anderson, C. Erikson., “Piezoelectric properties of dry and wet bone”; J Nature Vol 227 August 1 1970.
19. Bromage TG, Goldman HM, McFarlin SC, Warshaw J, Boyde A, Riggs CM., “Circularly polarized light standards for investigations of collagen fiber orientation in bone”. Anat Rec B: New Anat 2003; 274(1): 157 – 68.
20. Shijie Wu., “Piezoresponse Force Microscopy”, Application Note, Agilent Technologies.
21. Catalin Hamagea et al., “Two – dimensional nanoscale structural and functional imaging in Individual collagen type I fibrils”. J Biophysics, Volume 98, June 2010, p. 3070 – 3077.
22. Karem Noris – Suarez et al., “In Vitro deposition of hydroxyapatite on cortical bone collagen stimulated by deformation – induced piezoelectricity”, J Biomacrmolecules 2007, 8, 941 – 948.
23. Ingomar Jager and Peter Fratzl., “Mineralized collagen fibrils: A mechanical model with a staggered arrangement of mineral particles”. J Biophysics, Volume 79, October 2000, p.1737 – 1746.
24. Peter Fratzl and Richard Weinkamer., “Nature’s hierarchical materials”, Progress in Materials Science, Volume 52, Issue 8, November 2007, Pages 1263 – 1334.
25. Jean – Yves Reginster and Nansa Burlet., “Osteoporosis: A still increasing prevalence”, Bone 38 (2006) S4 – S9.
26. Andrea Kwaczala (2012) *Alendronate and PTH Differentially Modulate Bone Quality and Reduce Adiposity in an OVX Rat Model.* Unpublished PhD Thesis. Stony Brook University.
27. Petar Milovanovic et al., “Nanostructure and mineral composition of trabecular bone in the lateral femoral neck: Implications for bone fragility in elder women”. Acta Biomaterialia 7 (2011) 3446 – 3451.

28. A.A. Gaidash et al., “Nanoporous Structure of bone matrix at osteoporosis from data of Atomic Force Microscopy and IR spectroscopy”, Journal of osteoporosis, Volume 2011, Article ID 162041, 7 pages.
29. Z.Q. Peng et al., “Long term effects of ovariectomy on the mechanical properties and chemical composition of rat bone”, J Bone, Vol.20, No.3, March 1997: 207 – 212.